Respective Roles of the Guinea Current and Local Winds on the Coastal Upwelling in the Northern Gulf of Guinea

S. DJAKOURÉ

Laboratoire de Physique de l'Atmosphère et de Mécanique des Fluides, UFR SSMT, Université Félix Houphouët-Boigny, Abidjan, Côte d'Ivoire, and International Chair of Mathematical Physics and Applications (ICMPA-UNESCO Chair), University of Abomey-Calavi, Cotonou, Benin

P. PENVEN

Laboratoire d'Océanographie Physique et Spatiale, UMR 6523 CNRS/IFREMER/IRD/UBO, Plouzané, France

B. BOURLÈS

Laboratoire d'Études en Géophysique et Océanographie Spatiales, UMR 5566 CNES/CNRS/IRD/UPS, Plouzané, France, and International Chair of Mathematical Physics and Applications (ICMPA-UNESCO Chair), University of Abomey-Calavi, Cotonou, Benin

V. KONÉ

Centre de Recherches Océanologiques, Abidjan, Côte d'Ivoire

J. VEITCH

South African Environmental Observation Network, Egagasini Node, Cape Town, South Africa

(Manuscript received 26 May 2016, in final form 20 March 2017)

ABSTRACT

The northern Gulf of Guinea is a part of the eastern tropical Atlantic where oceanic conditions due to the presence of coastal upwelling may influence the regional climate and fisheries. The dynamics of this coastal upwelling is still poorly understood. A sensitivity experiment based on the Regional Oceanic Modeling System (ROMS) is carried out to assess the role of the detachment of the Guinea Current as a potential mechanism for coastal upwelling. This idealized experiment is performed by canceling the inertia terms responsible for the advection of momentum in the equations and comparing with a realistic experiment. The results exhibit two major differences. First, the Guinea Current is found to be highly sensitive to inertia, as it is no longer detached from the coast in the idealized experiment. The Guinea Current adjusts on an inertial boundary layer, the inertial terms defining its lateral extension. Second, the upwelling east of Cape Palmas disappears in absence of the Guinea Current detachment. This is in contrast with the upwelling east of Cape Three Points, which is still present. The results suggest that two different generation processes of the coastal upwelling need to be considered: the upwelling east of Cape Palmas (which is due to inertia, topographic variations, and advective terms effects resulting in important vertical pumping) and the upwelling east of Cape Three Points (which is principally induced by local winds). In addition to recent work ruling out the role of eddies, this study clarifies the processes responsible for this coastal upwelling.

1. Introduction

The northern Gulf of Guinea is known to host a coastal upwelling in boreal summer (Varlet 1958; Philander 1979; Hardman-Mountford and McGlade 2003). This cooling process appears seasonally, between Nigeria and Côte d'Ivoire, along the northern coast of the Gulf of Guinea. It presents two main upwelling cells: downstream of Cape Three Points (4°44′N, 2°05′W) and downstream of Cape Palmas (4°22′N, 7°43′W) (Lemasson and Rébert 1973; Arfi et al. 1991; Koranteng and McGlade 2001; Hardman-Mountford and McGlade 2003).

Corresponding author: Sandrine Djakouré, agre.djakoure@ird.fr

DOI: 10.1175/JPO-D-16-0126.1

As expected, coastal upwelling in the northern Gulf of Guinea drives the productivity of the marine ecosystems. Zooplankton biomass (Wiafe et al. 2008) as well as fishery productivity (Cury and Roy 2002) are directly linked to the major upwelling season. In addition, previous studies have shown that upwelled colder waters could also modulate the amplitude of the African monsoon, illustrating the potential role of coastal upwelling on regional climate (Opoku-Ankomah and Cordery 1994; Gu and Adler 2004).

Coastal upwelling is known to be generated by several mechanisms where the most important is the wind-induced coastal divergence (Bakun and Nelson 1991). Indeed, when the winds are upwelling favorable, an offshore Ekman transport is created and cold, nutrients-rich deep waters are upwelled to the surface. This is the case of the four major eastern boundary coastal upwelling systems (the Humboldt, California, Canary, and Benguela Current systems; Wooster and Reid 1963; Schumann et al. 1982; Enriquez and Friehe 1995; Marchesiello et al. 2003; Penven et al. 2005; Gruber et al. 2011).

Besides this main cause, other processes such as Ekman pumping (Enriquez and Friehe 1995), coastline disturbances (Crépon et al. 1984; Durski et al. 2008), changes in shelf width (Pringle 2002; Allen and Hickey 2010), or topography variations (Hsueh and O'Brien 1971; Janowitz and Pietrafesa 1982; Veitch et al. 2010) may be involved to explain coastal upwelling. For example, the works of Hsueh and O'Brien (1971) suggested that friction motion in the interior ocean, due to the presence of an alongshore current, may transport bottom Ekman flux on the continental shelf, which would induce coastal upwelling. Veitch et al. (2010), by using a numerical model, found that the upwelling cells of the Benguela system are enhanced downstream of capes because of the variation of the coastline and the topography.

Many studies have been made on the interactions between flow and coastline topography such as upwelling generated past capes (Crépon et al. 1984; Boyer and Tao 1987; Penven et al. 2000; Djakouré et al. 2014). From the experimental study of Boyer and Tao (1987), it appears that nondimensional numbers predict the generation of cyclonic eddies downstream of capes, according to the location of the cape (on the right or left side of the flow and for poleward or equatorward currents along an eastern boundary). Cyclonic eddies are supposed to generate upwelled cold waters. Following the study of Boyer and Tao (1987), Djakouré et al. (2014) have found, in the Gulf of Guinea, a cyclonic eddy shedding regime. However, these authors have shown, from an idealized straight coastline experiment, that coastal upwelling is still present even without capes and cyclonic eddies, rejecting the hypothesis of the role of these eddies for coastal upwelling.

In the Gulf of Guinea, the four main hypotheses that have been put forward to explain the presence of the Gulf of Guinea coastal upwelling are as follows:

1) The dynamical upwelling processes associated with the presence at the coast of the eastward-flowing Guinea Current (GC). The Guinea Current is in geostrophic balance and associated with a rise of the thermocline toward the surface from the west to the east (Ingham 1970; Bakun 1978; Colin 1988; Colin et al. 1993). Ingham (1970) suggested that the geostrophic adjustment of Guinea Current and the Ekman transport are the causes of the coastal upwelling. However, Philander (1979), by using a two-dimensional, simplified, oceanic model, showed that the amplitude of the upwelling induced by the Guinea Current is negligible compared to the observations.
   The study of Colin (1988), based on in situ measurements of the French program Ocean and Climate in the equatorial Atlantic (FOCAL), off the Ivory Coast between 1983 and 1984, showed that the variability of SST is closely related to the intensity and the extension in latitude of the Guinea Current. The thermocline is much closer to the surface at the coast in summer, when the Guinea Current is found off the continental shelf and not confined only on the continental shelf.
2) The vertical pumping by cyclonic eddies generated downstream of the major capes (Marchal and Picaut 1977; Binet 1997). Marchal and Picaut (1977) analyzed the surface isotherms between Ghana and the Ivory Coast, from cruise campaigns carried out between 1973 and 1974. The closed isotherms' contours observed east of Cape Palmas and Cape Three Points, where SST minima are observed in boreal summer, suggest the presence of cyclonic eddies downstream of these capes. Binet (1997) is also in favor of this hypothesis. However, according to this last author, the cyclonic eddies hypothesis must be verified by other observations and model. Djakouré et al. (2014) confirmed the presence of trapped cyclonic eddies downstream of capes. Theses cyclonic eddies have been found to be generated by interactions between capes and the Guinea Current. However, as mentioned previously, Djakouré et al. (2014) have shown that coastal upwelling is still present without these cyclonic eddies rejecting this hypothesis.
3) The Ekman pumping caused by wind stress curl. Colin (1991) has put forward the wind stress curl as

another additive possible mechanism. This influence between SST and wind stress curl was first suggested by the works of Katz and Garzoli (1982) and Garzoli and Katz (1983) and also by Philander and Pacanowski (1986) from the outputs of a tropical Atlantic model forced by climatology wind, from 1982 to 1984.

4) The remote influence of the equatorial ocean through the propagation of equatorial Kelvin waves, generating coastal-trapped waves along the African coast (Moore et al. 1978; Clarke 1979; Servain et al. 1982; Picaut 1983). Using a linear model, Moore et al. (1978) found that an accumulation of surface waters is observed along the Brazilian coast after an intensification of the trade winds in the western basin. A zonal pressure gradient is settled in to compensate the force due to the wind stress. This results in a spread of equatorial Kelvin waves from west to east and coastal-trapped waves along the African coast. It is followed by a rise of the thermal structure at the equator and in the Gulf of Guinea. This rise spreads the slope of the thermocline and generated coastal upwelling. Picaut (1983) also supported this theory but advocated that more measurements and other analysis of the thermal structure with model's surface need to be done before fully validating this hypothesis.

A combination of all these causes has also been proposed (Colin 1988; Roy 1995). Because Djakouré et al. (2014) have already been able to rule out the cyclonic eddies generated downstream of capes as a cause of coastal upwelling, the focus of this paper will be on another possible upwelling cause: the influence of the detachment of the Guinea Current.

In this paper, we use a numerical model to test the influence of the detachment of the Guinea Current as a potential cause of coastal upwelling in the northern Gulf of Guinea. Flowing eastward all year long with surface current speeds of about 50 cm s^{-1} and a thickness of about 30 to 40 m deep, the Guinea Current is the principal current of the northern Gulf of Guinea (Longhurst 1962; Ingham 1970). The Guinea Current is flowing along the western African coast between 2° and 5°N (approximately 200 km in width). Considered an extension of the North Equatorial Countercurrent (NECC), the Guinea Current transport is minimum in boreal winter and maximum in summer, with velocities reaching 100 cm s^{-1}. Note that the boreal summer corresponds to the major upwelling season (Richardson and Walsh 1986; Arnault 1987; Richardson and Reverdin 1987). The average transport of the Guinea Current has been estimated at about 2 to 5 Sv (1 Sv $\equiv 10^6$ m^3 s^{-1}) by Kolodziejczyk (2008).

Dynamical upwelling associated with current detachment can be an efficient process for coastal upwelling. Such a process has been observed, for example, inshore of the East Madagascar Current, at the southern tip of Madagascar (Machu et al. 2002). Inertia is key for current detachment (Chao et al. 1996; Özgökmen et al. 1997). Using a numerical model, José (2013) and José et al. (2016) have shown explicitly that the upwelling south of Madagascar is induced by the detachment of the East Madagascar Current. In a model simulation where the terms responsible for the advection of momentum (the inertia) have been canceled, the East Madagascar Current remains attached to the continental shelf and the upwelling cell south of Madagascar vanishes. The cancellation of advection of momentum can be seen as a linearization of the momentum equations for a low Rossby number. The absence of advection of momentum in a primitive equations model prevents the detachment of currents as well as the occurrence of eddies. This latter characteristic has been used, for example, by Gruber et al. (2011) and José et al. (2016).

A methodology equivalent to the one described by Gruber et al. (2011) and José et al. (2016) is used in the present study, which is a continuity of the work of Djakouré et al. (2014). To determine if the Guinea Current detachment is the cause of coastal upwelling, we have conducted two simulations of a high-resolution ocean model of the region. We have compared a realistic simulation (where the upwelling is present and corresponds to observations) with an idealized experiment where the inertial effects are canceled. In addition, results from high-resolution local wind effects are also analyzed. Although the northern coast of the Gulf of Guinea is mainly zonally oriented, the Ghanaian coast to the east presents a slant that tends to align with the winds, favoring wind-driven upwelling (Adamec and O'Brien 1978; Toualy et al. 2012; Djakouré et al. 2014).

2. Methodology approach

a. Ocean model configuration for the Guinea Current

The ocean circulation model used is based on the Institut de Recherche pour le Développement (IRD) version of the Regional Oceanic Modeling System (ROMS; Shchepetkin and McWilliams 2003, 2005). ROMS solves the primitive Navier–Stokes equations with a free sea surface elevation and following the Boussinesq and hydrostatic approximations.

ROMS has been first conceived for the study of coastal and regional oceanic processes at high resolution, such as coastal upwelling, using a generalized,

terrain-following, vertical coordinate (Marchesiello et al. 2003; Marchesiello and Estrade 2009; Veitch et al. 2009; Marchesiello and Estrade 2010). Such a topography-following coordinate allows a better representation of coastal processes and topographic effects (Song and Haidvogel 1994).

The model is based on higher-order numerical schemes. A third-order upwind advection scheme is split into a centered fourth-order advection operator and a rotated biharmonic diffusion operator with flow-dependent hyperdiffusivity to improve the conservation of water masses properties (Marchesiello et al. 2009). A K-profile parameterization (Large et al. 1994) is used for the parameterization of the unresolved turbulence.

To maintain the model stability and suppress spurious reflections, a mixed passive–active radiation scheme with adaptive nudging and sponge layers (Marchesiello et al. 2001) are used for the lateral boundaries of the large-scale parent domain. Explicit lateral viscosity is set to zero out of the sponge layers of 10 grid points, at the open boundaries of the parent grid, where it increases smoothly in order to prevent model inconsistencies (Marchesiello et al. 2001).

The IRD version of ROMS has a two-way nesting capability, which allows a large-scale grid to interact with a higher-resolution coastal grid (Blayo and Debreu 1999; Debreu and Blayo 2008; Debreu et al. 2012). The boundary conditions of the nested child grid are given by the parent grid, while the solution of the parent grid is updated by the high-resolution child grid. This two-way embedding methodology is based on the library Adaptive Grid Refinement in Fortran (AGRIF; Debreu et al. 2012).

This model configuration has been implemented to simulate the ocean circulation in the northern Gulf of Guinea. A complete description and evaluation of the configuration is given by Djakouré et al. (2014). The large-scale model configuration encompasses the tropical Atlantic at a horizontal grid resolution of 1/5° (approximately 22 km) with an embedded high spatial resolution grid in the Gulf of Guinea at 1/15° (approximately 7 km; Djakouré et al. 2014). A configuration of the Guinea Current system should take into account the whole basin to allow for equatorial Kelvin waves generated after a change in trade winds off the Brazilian coast to influence the coastal upwelling. It should also include the major currents of the area of interest (Servain et al. 1982; Picaut 1983; Djakouré et al. 2014). The model domain extends from 65°W to 15°E in longitude and from 10°S to 14°N in latitude for the parent grid (Fig. 1a). The child grid extends from 12°W to 12°E in longitude and from 4°S to 8°N in latitude (the black box in Fig. 1b).

The model is run for 10 years, forced by the monthly wind stress from the Scatterometer Climatology of Ocean Winds (SCOW) at the surface (Risien and Chelton 2008) and by the *World Ocean Atlas 2009* (*WOA09*) monthly climatology at the open boundaries. The surface heat and freshwater fluxes are derived from the monthly climatology of the Comprehensive Ocean–Atmosphere Data Set (COADS; Da Silva et al. 1994). The ability of this configuration to correctly reproduce the ocean dynamics such as the mean state and the seasonal cycle of the known ocean circulation has been addressed by Djakouré et al. (2014).

b. Idealized experiment

In the present study, we investigate the effects of the detachment of the Guinea Current on the coastal upwelling in the northern Gulf of Guinea. To do so, we compare the realistic model experiment described above (used as a reference) with an idealized experiment (called NogradU), in which the terms responsible for the detachment of the Guinea Current have been canceled. These terms are the nonlinear advection terms in the horizontal momentum balance highlighted by a brace on the left-hand side of Eqs. (1) and (2):

$$\frac{\partial u}{\partial t}+\overbrace{u\frac{\partial u}{\partial x}+v\frac{\partial u}{\partial y}+w\frac{\partial u}{\partial z}}=-\frac{1}{\rho_o}\frac{\partial P}{\partial x}+fv+\frac{\partial}{\partial z}K_v\frac{\partial u}{\partial z}+\overbrace{D_u}, \tag{1}$$

$$\frac{\partial v}{\partial t}+\overbrace{u\frac{\partial v}{\partial x}+v\frac{\partial v}{\partial y}+w\frac{\partial v}{\partial z}}=-\frac{1}{\rho_o}\frac{\partial P}{\partial y}-fu+\frac{\partial}{\partial z}K_v\frac{\partial v}{\partial z}+\overbrace{D_v}, \tag{2}$$

where x, y, and z (m) are, respectively, the zonal, meridional, and vertical directions in the Cartesian coordinate system; u and v ($\mathrm{m\,s^{-1}}$) are the zonal and the meridional components of the flow; t (s) is the time; ρ_o ($1025\,\mathrm{kg\,m^{-3}}$) is the reference density; P ($\mathrm{kg\,m^{-1}\,s^{-2}}$) is the pressure; f ($\mathrm{s^{-1}}$) is the Coriolis parameter; and K_v ($\mathrm{m^2\,s^{-1}}$) the vertical coefficient of turbulent viscosity. As common practice for regional modeling with ROMS, no explicit horizontal turbulent viscosity is added in the momentum equations (Marchesiello et al. 2003; Gruber et al. 2011). We rely on the limited dissipation associated with the third-order upstream advection scheme for the dissipation at grid scale. This is represented by the terms D_u and D_v in Eqs. (1) and (2). When canceling the advection of momentum, this small-scale dissipation is removed as well as the eddy cascading by nonlinear interactions (Gruber et al. 2011). For consistency, we did not reintroduce any explicit viscosity to compensate for this lack of dissipation in the NogradU experiment. This could result in some numerical grid-level noise for the velocities (Gruber et al. 2011). The resulting linearized equations of momentum are

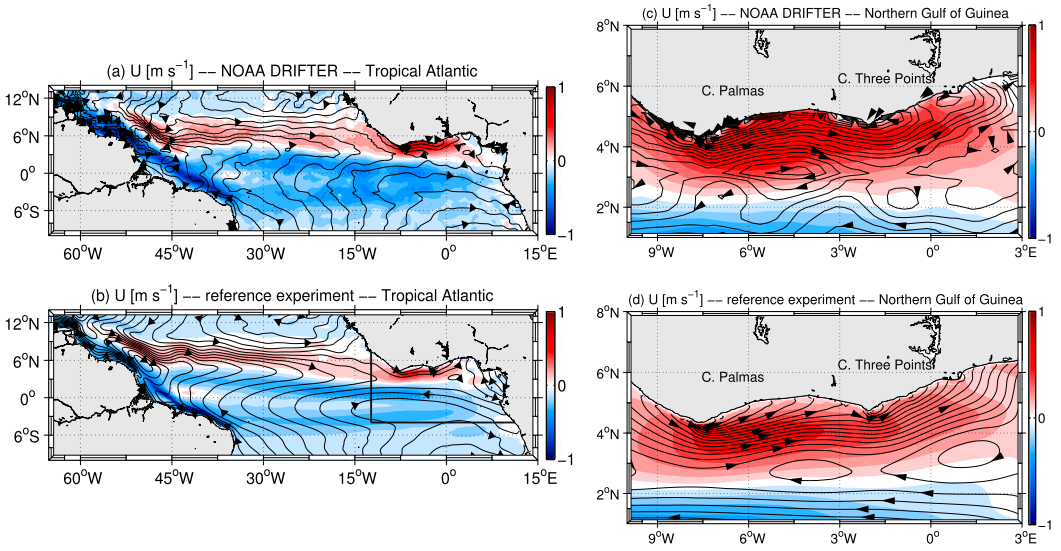

FIG. 1. Maps of the spatial distribution of the annual-mean zonal velocity U (m s^{-1}) in the tropical Atlantic for (a) NOAA's drifters and (b) the idealized experiment. The contour interval is 0.1 m s^{-1}. The black box in (b) delineates the child domain. As in (a),(b), but in the northern Gulf of Guinea for (c) NOAA's drifters and (d) the idealized experiment. The contour interval is 0.1 m s^{-1}. The mean SSHs (cm) representing the surface geostrophic circulation [contour intervals are 2 cm in (a) and (b) and 0.5 cm in (c) and (d)] are superimposed in black solid lines for (left) AVISO observations and (right) the reference experiment.

integrated with the other equations of the model, all the parameters being kept identical as in the reference experiment. The comparisons are based on model outputs from years 5 to 10 for both simulations.

c. *Wind-driven upwelling*

Although coastal upwelling in the northern Gulf of Guinea cannot be explained at large scale by offshore Ekman transport (Bakun 1978), an analysis is made to determine whether smaller-scale wind structures could affect the cooling in coastal regions. Ekman transports responsible for wind-driven coastal upwelling are calculated from the formula of Bakun (1973) [Eq. (3)]:

$$E_k = -\frac{\tau_{\text{alongshore}}}{\rho_o f}, \tag{3}$$

where E_k is the offshore Ekman transport per unit of coastline (m^3 s^{-1} m^{-1}) and $\tau_{\text{alongshore}}$ is the alongshore wind stress component (N m^{-2}) extracted from the monthly wind stress SCOW (Risien and Chelton 2008).

d. *Datasets*

In situ measurements and satellite products are used for comparisons with the reference model simulation. We use two independent datasets for the SST annual-mean and seasonal variations:

1) the Commonwealth Scientific and Industrial Research Organization (CSIRO) Atlas of Regional Seas 2009 (CARS; Dunn and Ridgway 2002), gridded on a global grid at a resolution of ½° (www.cmar.csiro.au/cars); and
2) the Moderate Resolution Imaging Spectroradiometer (MODIS) from the *Terra* satellite of the National Aeronautics and Space Administration (NASA), at 4-km horizontal spatial resolution. (These data are available at http://oceandata.sci.gsfc.nasa.gov.)

The near-surface velocities from the Global Drifter Center of the National Oceanic and Atmospheric Administration (NOAA; www.aoml.noaa.gov/phod/dac/dacdata.html), gridded at a ½° × ½° resolution (Lumpkin and Johnson 2013), are compared with the model mean surface circulation.

Furthermore, the sea surface height (SSH) satellite altimeter products produced by AVISO (www.aviso.altimetry.fr) are used to evaluate the model SSH and derived circulation. This dataset is interpolated on a ¼°-resolution grid and covers the period from 14 October 1992 to 27 December 2011 (Ducet et al. 2000).

3. Results and analysis

a. *Model and data comparisons*

The ability of the model to accurately simulate the ocean dynamics of the tropical Atlantic and the Gulf of

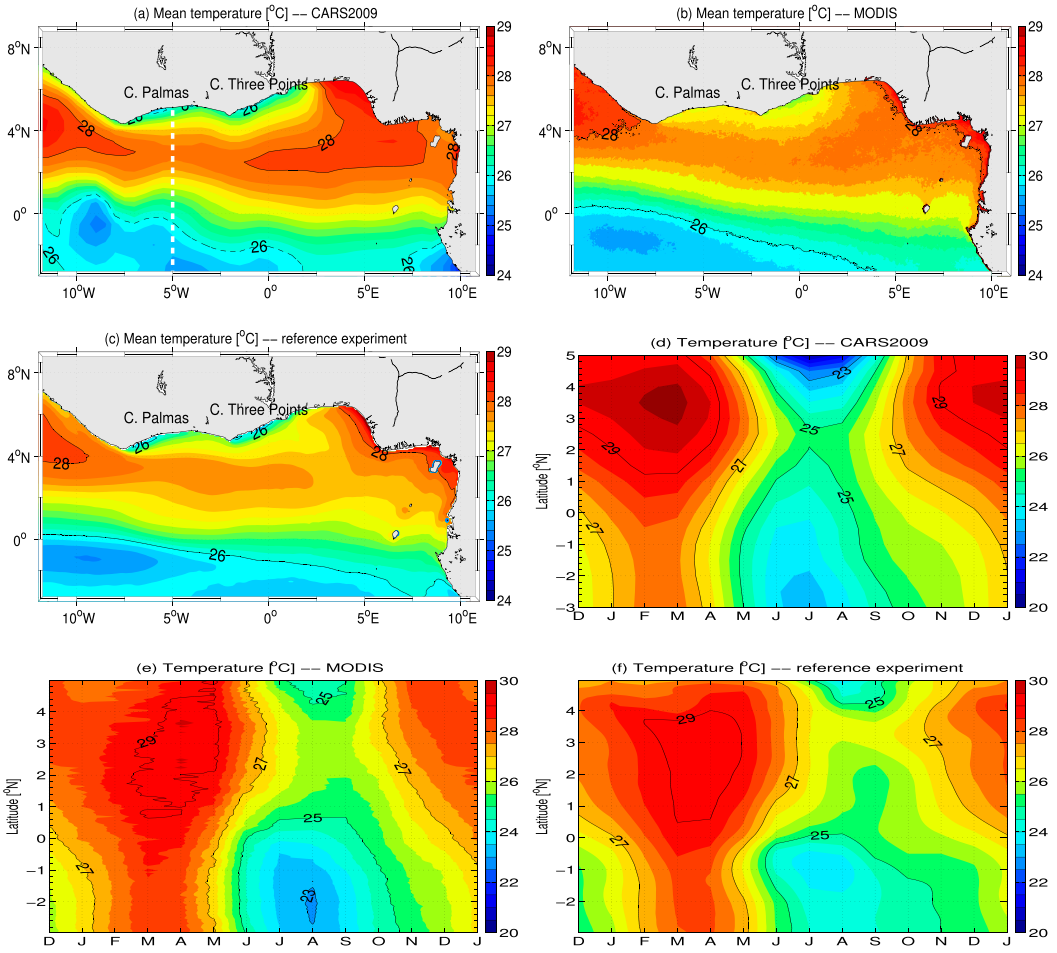

FIG. 2. Maps of the spatial distributions of the annual-mean SST (°C) in the northern Gulf of Guinea for (a) CARS, (b) MODIS, and (c) the reference experiment. The contour interval is 0.2°C. Time–latitude diagrams of sea surface temperature (°C) at 5°W, between 5°N and 3°S, for (d) CARS, (e) MODIS, and (f) the reference experiment. The location of the transect is represented by the white dashed line in (a). The contour interval is 0.5°C. The time axis in months extends from December to January.

Guinea Currents system (left and right panels in Fig. 1) has been already supported by Djakouré et al. (2014). In addition, to evaluate the configuration capability in reproducing the coastal upwelling features, the SSTs are presented in Fig. 2 for CARS, MODIS, and the reference experiment.

1) SURFACE OCEAN CIRCULATION

Figure 1 illustrates the mean characteristics of the surface currents in the tropical Atlantic (Figs. 1a,b) and the northern Gulf of Guinea (Figs. 1c,d). The zonal velocities are represented by the NOAA drifter climatology (top panels; Lumpkin and Johnson 2013) and the reference model (bottom panels). The annual-mean SSH, representing the mean geostrophic surface circulation, is also shown for the observed mean dynamic topography (top panels; Rio et al. 2011) and for the reference model (bottom panels).

The annual-mean zonal velocities in the tropical Atlantic for the reference experiment have already been evaluated against the NOAA drifter climatology by Djakouré et al. (2014), with satisfactory results (Figs. 1a,b). The main zonal components of the tropical current system (Bourlès et al. 1999; Schott et al. 2004) are illustrated: the westward North Brazilian Current (NBC) along the Brazilian coast, the westward South Equatorial Current (SEC) flowing between 2°S and 2°N, the eastward NECC located between 4° and 11°N, and the Guinea Current along the coast and north of 2°N. The SSH contours and the derived circulation for the model are also comparable with the observations.

In the northern Gulf of Guinea (Figs. 1c,d), the northern branch of the SEC is located around 2°N, with

comparable velocities for both observed and simulated data. On the other hand, the SSH contours representing the geostrophic current streamlines of the SEC simulated by the model are slightly more tightened than the observed ones. The observations and the model both show that the Guinea Current is flowing eastward between 2°N and the African coast with an average velocity of about $0.5\,m\,s^{-1}$. For both the model and observations, the mean alongshore extension of the Guinea Current velocity core ranges approximately from 9°W to 3°E. They also both agree on the width of the current of about 200 km. However, the simulated Guinea Current maximum velocity is slightly lower in intensity by approximately $0.1\,m\,s^{-1}$. The meandering structure of the Guinea Current is noticeable on the annual-mean sea surface height for both the model and observations (Figs. 1c,d). This confirms the representation by the reference experiment of the mean aspects of the Guinea Current in terms of width, path, and amplitude.

2) SST ANNUAL-MEAN AND SEASONAL VARIABILITY

Figure 2 presents the spatial distribution of the annual-mean surface temperature, in the Gulf of Guinea, for the climatology CARS (Fig. 2a), MODIS satellite products (Fig. 2b), and the reference experiment (Fig. 2c). The general characteristics of SST are found in both the observations and the model. For each product we observe three different areas: (i) a wide, colder band between 2°N and 3°S, with temperatures below 25°C; (ii) a warmer zone with temperatures of about 27.5°C, between 2°N and about 4°N (extending farther north in the northwest and the northeast); and (iii) a colder area with temperature of 26.5°C on average, along the northern coast of the Gulf of Guinea, between 7°W and 3°E.

The model simulation captures the coastal signature of upwelling seen in CARS: a local SST minimum east of both Cape Palmas and Cape Three Points, as described in previous studies (Koranteng and McGlade 2001; Hardman-Mountford and McGlade 2003). Although there are good correspondences for the colder SST along the coast for CARS and the reference experiment, MODIS temperatures are warmer along the coast (about 1°C).

The last three panels in Fig. 2 depict the seasonal variability of SST. These are time–latitude diagrams of SST extracted along 5°W, between 5°N and 3°S, for CARS climatology (Fig. 2d), MODIS satellite product (Fig. 2e), and the model simulation (Fig. 2f). The observed seasonal cycle of SST is in general well reproduced by the model. The known features of the warm and cold seasons of this seasonal cycle are present. From the end of December to March, a minor cold season is shown between 5°N and 4°N, with temperatures of about 27.5°C for MODIS and the model. This minor cooling is not depicted by CARS, which exhibits temperatures up to 29°C. Both simulated and observed SSTs present a major warm period between February and May, with maximum temperatures of about 29°C for MODIS and the model and 30°C for CARS. However, the warm peak for CARS occurs between February and March, 1 month in advance compared to MODIS and the model. A major cold period is observed from July to September. A minor warm period is shown at the end of October. During this latter, the temperatures for MODIS and the model are 28°C, while CARS temperatures reach 29°C. Note that CARS is slightly warmer (<1°C) during the warm seasons than MODIS and the model. These differences are within the range of differences between in situ and satellite observations reported for other upwelling systems (Dufois et al. 2012). The SST minimum is reached in July for CARS, at around 5°N, with a value of 21°C. CARS depicts the coldest minimum. The SST minimum is reached in August for MODIS and the model. However, as this minimum value of 23°C is reached at around 2°S for MODIS, a slight warm bias of 1°C in the model can be seen. Moreover, the described seasonal cycle is similar to that shown by Jouanno et al. (2011, their Fig. 1b), obtained from a ¼°-resolution NEMO ocean model and the satellite product Tropical Rainfall Measuring Mission (TRMM) Microwave Imager (TMI).

To summarize, the mean modeled structure of the Guinea Current is comparable with observations, and also the annual mean and seasonal cycle in SST are reproduced by the reference experiment with a signature of coastal upwelling. Along with the previous comparisons made by Djakouré et al. (2014), these elements support the idea that this model is suitable for addressing the processes responsible for coastal upwelling in the Gulf of Guinea.

b. *Effects of local winds on coastal upwelling*

Along the coast of the Gulf of Guinea, by using a wind stress climatology at a resolution of 1°, Bakun (1978) has shown that the maximum in Ekman transport divergence in boreal summer does not coincide with the minimum in SST but is located farther to the east. Nevertheless, Colin (1988) suggested that wind effects (Ekman divergence and pumping) should still be taken into account, especially east of Cape Palmas. Here, a higher-resolution wind stress climatology (SCOW) is used to revisit the effects of local wind as a driver for coastal upwelling. By using Eq. (3), we estimate the Ekman transport associated

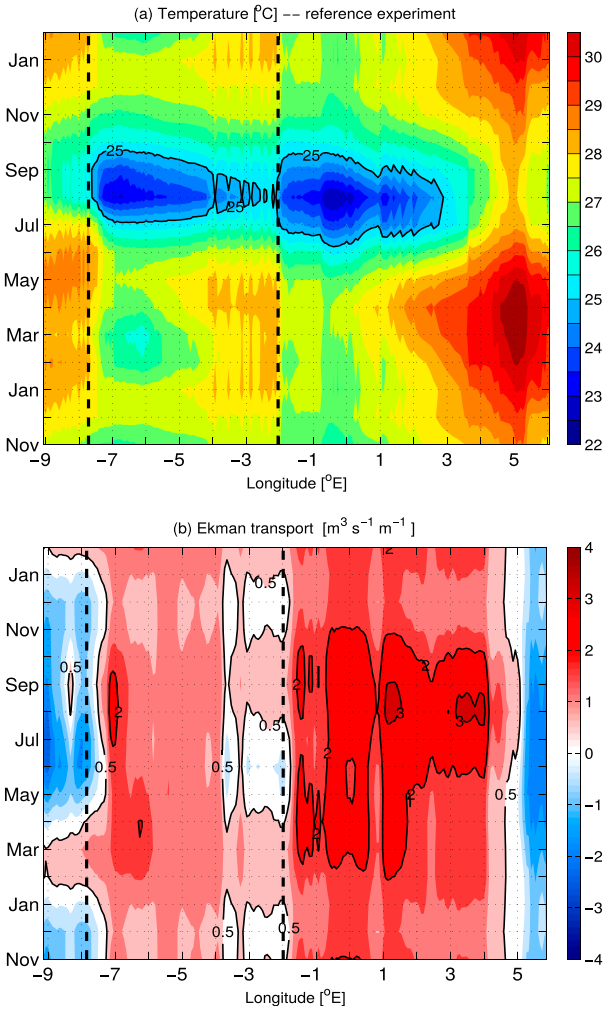

FIG. 3. Hovmöller longitude–time diagrams of (a) the reference experiment SST (°C) and (b) the Ekman transport ($m^3\,s^{-1}\,m^{-1}$), inducing coastal divergence in the northern Gulf of Guinea, between 9°W and 6°E, at the coast (the first grid points in the ocean are around 7 km). The contour interval is 0.5°C in (a) and 0.5 $m^3\,s^{-1}\,m^{-1}$ in (b). The dashed black line at 7.7°W (2°W) represents the longitude of Cape Palmas (Cape Three Points). The time axis in months extends from November to February.

with Ekman transport divergence (generated by alongshore wind stress).

Figures 3a and 3b depict the seasonal variability of SST for the reference experiment (Fig. 3a) and of Ekman transport (Fig. 3b) along the northern coast of the Gulf of Guinea (the first grid points in the ocean: around 7 km), between 9°W and 6°E. The isotherm 25°C is chosen as a threshold for the signature of coastal upwelling. This value is chosen for the upwelling in the eastern equatorial Atlantic because it is lower than the average SST observed in June in this area (Bakun 1978; Picaut 1983; Hardman-Mountford and McGlade 2003; Caniaux et al. 2011).

Between June and October, a band of colder waters extends between 7.7°W and 3°E as a clear signature of the major coastal upwelling (Fig. 3a). Colder waters are observed from early June around 0°, east of Cape Three Points, and from July around 7°W, east of Cape Palmas. For both regions, the SST reaches a minimum value of 23°C in August. We note that the cold waters signal, with SST lower than 23°C, decreases in duration and amplitude from Cape Palmas to Cape Three Points. The signal regains strength east of Cape Three Points and decreases again farther east. The simulated SST exhibits also a secondary minimum along the coast from February to March, more visible around 6°W. This corresponds to the minor cold season of upwelling in the northern Gulf of Guinea (Hardman-Mountford and McGlade 2003; Toualy et al. 2012).

The Ekman transport is positive throughout the year expected from November to January and May to July, between 4°W and the Cape Three Points (Fig. 3b). In general, it increases from west to east (from 0.2 to 3 $m^3\,s^{-1}\,m^{-1}$ around 1.5° and 3°E in August). During the major upwelling period, Ekman transport of about 0.2 to 2 $m^3\,s^{-1}\,m^{-1}$ is found between Cape Palmas and 7°W. From June, the Ekman transport east of Cape Three Points is greater than 2 $m^3\,s^{-1}\,m^{-1}$. A maximum value of 3 $m^3\,s^{-1}\,m^{-1}$ is reached in August, around 1.5° and 3°E. Note that the maximum values of Ekman transport are located east of the SST minimum values, as reported by Bakun (1978).

Correspondences between Ekman transport and SST are also noticeable during the minor upwelling season (March), as also shown by Bakun (1978). In fact, this minor upwelling appears to be associated with Ekman transport of 1.5 $m^3\,s^{-1}\,m^{-1}$ in March between 6° and 7°W.

Our results present some noticeable differences between Cape Palmas and Cape Three Points. While the Ekman transport is relatively large during both minor and major upwelling seasons east of Cape Three Points, it is much lower (below 2 $m^3\,s^{-1}\,m^{-1}$) during the major cold season east of Cape Palmas. To summarize, there are connections (as the highest value of Ekman transport is reached in August and the minimum value of upwelled SST is also observed during the same month) between the seasonal cycle of coastal SST and the Ekman divergence transport velocity east of Cape Three Points. This is not the case east of Cape Palmas during the major upwelling period. As described in the literature, wind-driven coastal upwelling cannot explain this event.

c. *Sensitivity study*

A sensitivity test is conducted to investigate the potential role of Guinea Current detachment as an alternative

mechanism for coastal upwelling east of Cape Palmas. In this section, the results of the NogradU experiment (i.e., the experiment in which advection of momentum is canceled but the tracers temperature and salinity advections are maintained) are compared with the outputs of the reference experiment.

1) Large-scale circulation and hydrology in the tropical Atlantic

(i) Large-scale circulation

To test if the large-scale circulation is still represented by the NogradU experiment, the spatial distribution of the annual-mean zonal velocity in the tropical Atlantic is shown in Figs. 4a and 4b for the reference (Fig. 4a) and NogradU (Fig. 4b) experiments. The known characteristics of the mean zonal circulation (Bourlès et al. 1999; Stramma et al. 2003) are represented in the reference experiment (Fig. 4a). In the western basin, the alongshore westward NBC is clearly shown with a maximum velocity of about $0.8\,\mathrm{m\,s^{-1}}$ (Fig. 4a). The northern (nSEC) and southern (sSEC) branches of the SEC are located on both sides of the equator (around 2°N and 2°S). The eastward NECC is flowing between 11° and 4°N and is connected with the Guinea Current in the Gulf of Guinea. The Guinea Current located along the African coast is the main surface current in our area of interest.

A large-scale zonal pattern showing westward velocities for the SEC at the equator and eastward velocities for the NECC and Guinea Current in the north is also present in NogradU, but the zonal velocities are generally higher (Fig. 4b). The SEC is located in the center of the basin, with an intensified northern branch ($0.2\,\mathrm{m\,s^{-1}}$) and a weaker northern extension. The NBC is still present along the Brazilian coast, but it is intensified and more coastally trapped. Numerical grid-scale noise can be seen along the western boundary between the equator and 6°S. As explained by Gruber et al. (2011) and José et al. (2016), for consistency, no explicit viscosity has been added to compensate for the lack of eddies in the NogradU experiment. This induces an enhanced numerical grid-level noise for the velocities at the western boundaries and, interestingly, a structure of alternating zonal jets for the NECC. As described by Gruber et al. (2011) and as can be seen in Fig. 4b, this numerical noise does not show an important impact on temperature and salinity.

Between 4° and 11°N, the NBC is still present with similar velocity values as in the reference experiment. The NECC structure is, however, different: in the NogradU simulation, this current is flowing in the form of westward zonal jets separated by zonal eastward jets, as observed around 7°N (Fig. 4b). We also note that the NECC velocity appears slightly lower, compared with the reference run. Despite these discrepancies, the NECC connection with the Guinea Current in the Gulf of Guinea can be observed in both simulations. The Guinea Current is present in the NogradU experiment, but it is now following closely the African coast in a narrower band (Fig. 4b).

These findings are also portrayed by the mean SSH and the derived surface circulation in the Gulf of Guinea, as shown in Figs. 4c and 4d for the reference and NogradU experiments, respectively. The large scale is relatively similar between the reference and NogradU simulations. Indeed, at the equator, the average circulation is almost similar. The North Atlantic (around 12°N) and South Atlantic (to 10°S) Gyres are also well presented.

The NECC is still observed in the NogradU experiment in the western basin. However, it is flowing in the form of westward zonal jets separated by zonal eastward jets, as mentioned above. Along the Brazilian coast, the tighter SSH contours depict the intensification of the NBC. Furthermore, the retroflection of the NBC is significantly marked. This result is expected because the retroflection process is dominantly inertial.

In eastern basin, the GC is still present but trapped at the coast. On the other side, the structure of the SEC is not really influenced, unlike the NECC and the GC.

(ii) Spatial distributions of surface salinity and temperature

No significant changes in the structure and magnitude of the annual-mean sea surface salinity is reported in the NogradU experiment (Fig. 5b), compared to the reference experiment (Fig. 5a). A slight difference is noted for the 35.5 isohaline, showing a more zonal extension at 6°N in the NogradU experiment. Also, around the NBC retroflection area between 8° and 4°N, the 34 isohaline presents a more meridional extension.

The spatial representation of SST during the major upwelling period [July–September (JAS)] is portrayed for the reference experiment (Fig. 5c) and the NogradU experiment (Fig. 5d). In absence of advection of momentum, tropical instabilities waves (TIWs) cannot be generated in NogradU. The TIWs contribute to warm up the cold water tongue (Menkès et al. 2002; Athié et al. 2009). Hence, the absence of TIWs and the presence of a stronger SEC (which might be related since TIWs could also transfer momentum) in the NogradU experiment result in colder SST at the equator and sharper fronts on its northern and southern flanks. At the equator, the 25°C isotherm is found at the east of 21°W for the

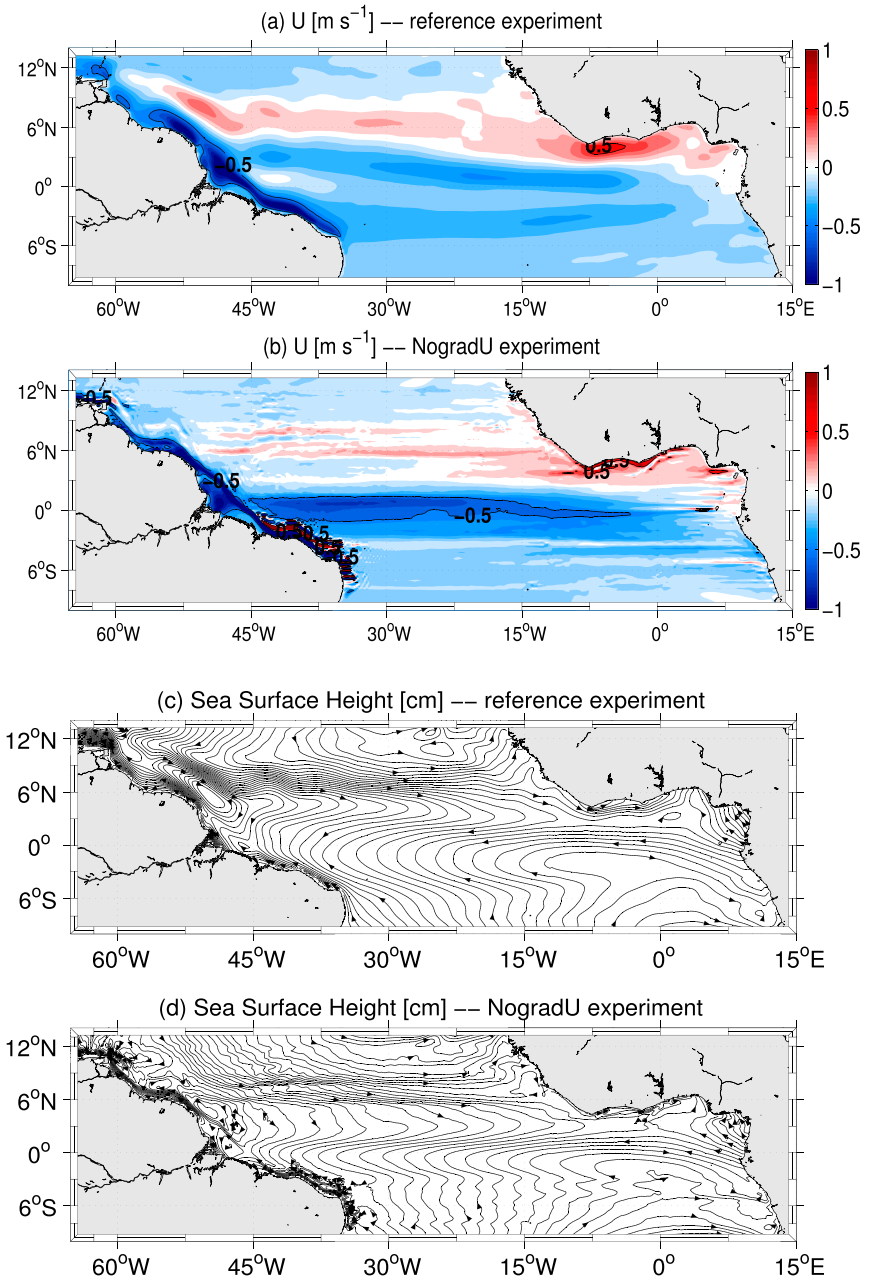

FIG. 4. Maps of spatial distribution of the annual-mean zonal velocity U in m s^{-1} in the tropical Atlantic for (a) the reference experiment and (b) the idealized experiment. The contour interval is 0.1 m s^{-1}. Map of the mean SSH (cm), representing the surface geostrophic circulation (contour interval is 1 cm) for (c) the reference experiment and (d) the idealized experiment.

reference simulation, while it extends to 31°W for NogradU.

Outside this equatorial band, differences in SST are weak between NogradU and the reference experiment. In the northern Gulf of Guinea, the 25°C isotherm, signature of coastal upwelling, is still present in the NogradU simulation to the east of Cape Three Points. The signature of coastal upwelling is no longer present in NogradU east of Cape Palmas.

(iii) Vertical structure of temperature

Figure 6 presents vertical temperature sections extracted at 10°W between 5°S and 5°N for the reference

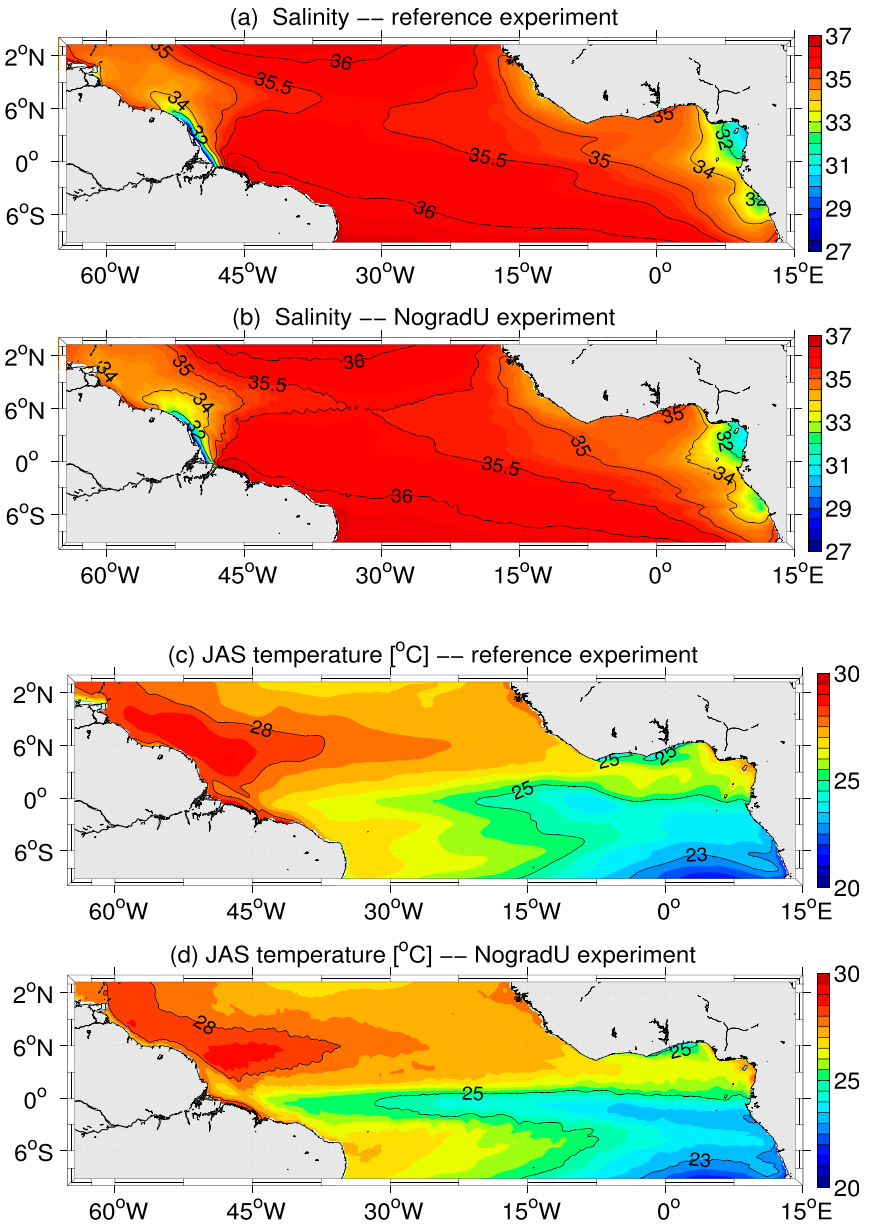

FIG. 5. Maps of the spatial distribution of the annual-mean salinity in the tropical Atlantic for (a) the reference experiment and (b) the idealized experiment. The contour interval is 0.1. Spatial distributions of the major cold season (JAS) of SST (°C) in the tropical Atlantic for (c) the reference experiment and (d) the idealized experiment. The contour interval is 0.5°C. The isotherms 23°, 25°, and 28°C are represented as black lines.

experiment (Fig. 6a) and the NogradU experiment (Fig. 6b). The isopycnal contours σ = 24.5, 25.5, 26.5, and 26.75 are superimposed. In general, the two vertical sections are relatively similar. A difference is noted for the 28°C isotherm at 4°N. This isotherm extends to 5°N in the NogradU experiment. Another difference in the σ = 26.5 and σ = 26.75 isopycnal depths can be observed north of 3°S; they are slightly deeper in the NogradU simulation. At the equator, the σ = 24.5 isopycnal in NogradU rises above 50 m, unlike the reference simulation, in agreement with the 26°C isotherm that is also closer to the surface. These differences in the structure of the vertical isotherms around the equator should be induced by differences in the Equatorial Undercurrent (EUC) structure and magnitude when the nonlinear terms

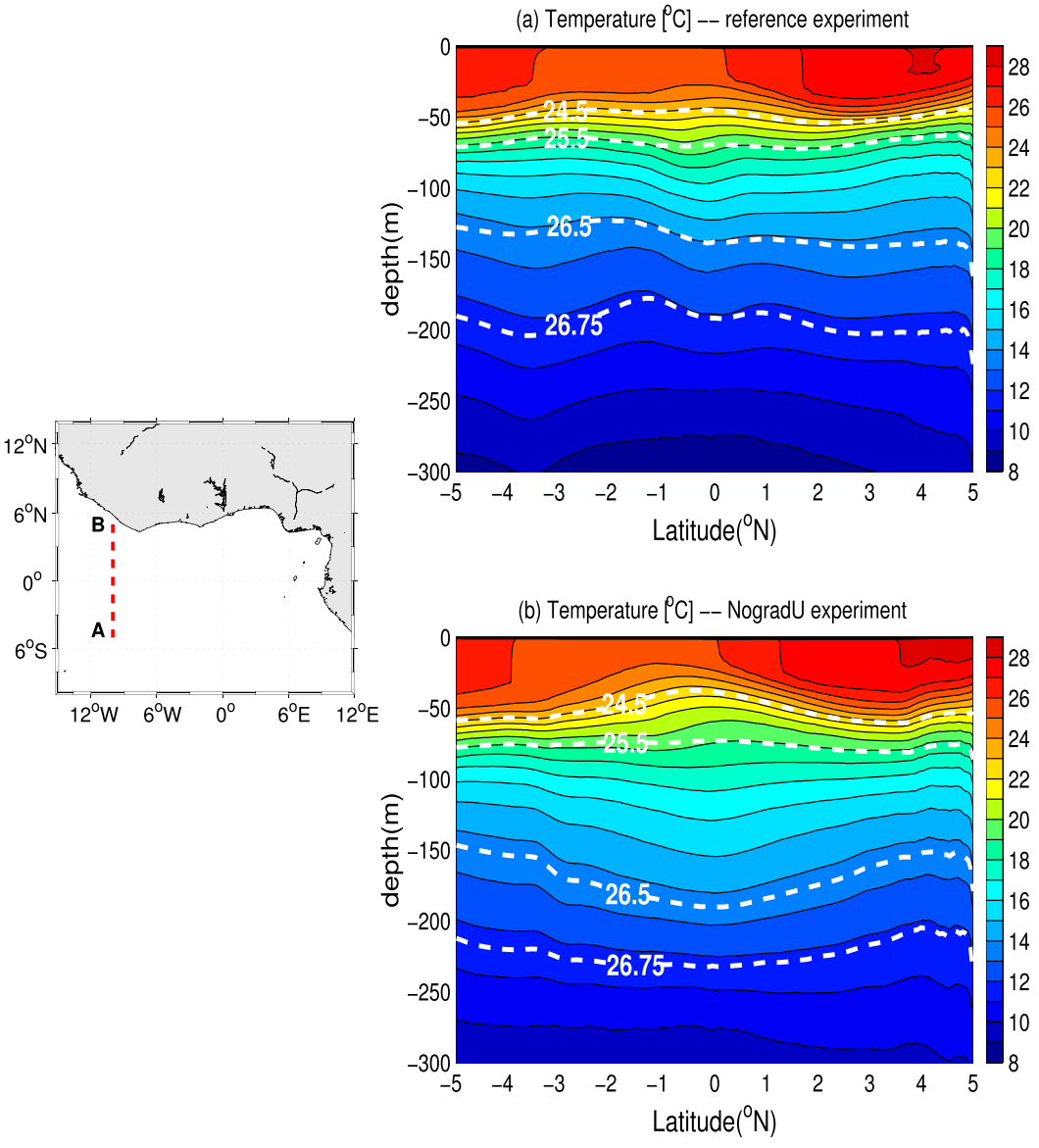

FIG. 6. Maps of the mean temperature (°C), at 10°W, between 5°S and 5°N, for the (a) reference experiment and (b) the idealized experiment. The location of the transect is represented in the left panel by the dashed red line, from A to B. The contour interval is 1°C. The white dashed lines represent the isopycnal contours σ = 24.5, 25.5, 26.5, and 26.75.

are set to zero (not shown). This is in agreement with the identification of a dependence of the EUC to inertial terms in the eastern basin by Wacongne (1989). Nevertheless, the EUC is not the subject of our study and does not influence our analysis and conclusions on the coastal upwelling.

In summary, despite having canceled the advection of momentum, the major features of the general circulation and hydrology in the NogradU experiment are in general preserved at large scale in the region of interest. This gives us confidence and allows us to study the dynamics of coastal upwelling through this sensitivity test. We will now focus on the northern Gulf of Guinea area.

2) Oceanic circulation and hydrology in the Gulf of Guinea

Effect of inertia on the Guinea Current

To illustrate the role of inertial terms on the Guinea Current dynamics, Figs. 7a and 7b show the annual-mean zonal currents (Fig. 7a) and the annual-mean SSH

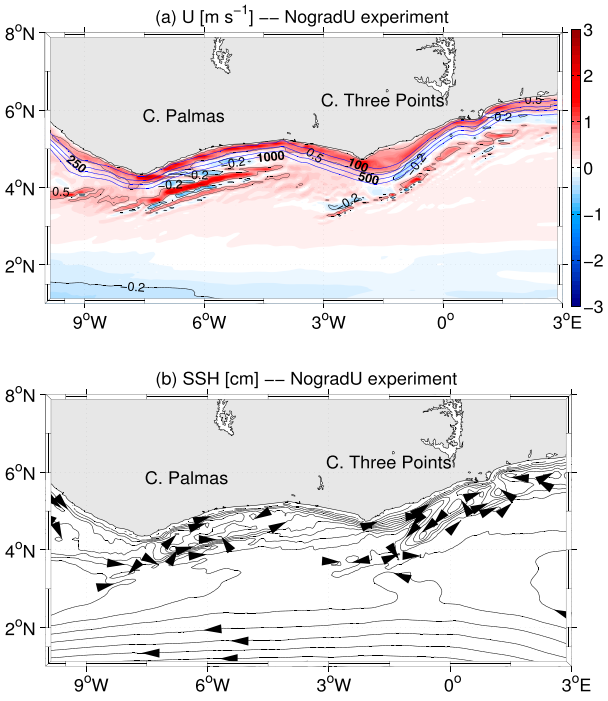

FIG. 7. (top) Annual-mean zonal velocity U ($m\,s^{-1}$) in the northern Gulf of Guinea for the idealized experiment. The contour interval is $0.1\,m\,s^{-1}$. The isobaths 100, 250, 500, and 1000 m are superimposed in blue lines. (bottom) Mean SSH (m) and derived surface circulation (0.5 cm contour interval) in the northern Gulf of Guinea for the idealized experiment. The flow direction is indicated by the arrows.

(Fig. 7b) for the NogradU experiment. The annual-mean zonal currents and the SSH for the reference experiment were described in section 3a(1) (Fig. 1d).

Although the Guinea Current is still present in NogradU experiment, it differs from the reference experiment through its spatial structure. For the reference experiment (Fig. 1d), the Guinea Current is flowing eastward between 2°N and the African coast on a width of approximately 200 km. A maximum velocity of about $0.6\,m\,s^{-1}$ is observed around 4°N, between 7.5° and 6°W. This current is stronger between 4°N and 3°N than at the coast. In NogradU (Fig. 7a), the Guinea Current is almost entirely confined in a narrow band between the coast and the topographic slope. The velocities are 3 times larger at the coast. A strong component is trapped at the coast and the continental shelf, with lower velocities south of 3°N. Similar changes in the Guinea Current structure are also evidenced through the annual-mean SSH (Fig. 7b).

Hence, in the realistic case, the scale defining the width of the Guinea Current appears to be controlled by advection of momentum. By analogy with previous work on western boundary currents (Charney 1955), we could suppose that the Guinea Current adjusts to the coast as an inertial boundary layer. In absence of inertia, the Guinea Current is still present but does not detach from the coast. Farther south, the nSEC spatial structure remains unchanged in absence of the advection of momentum.

3) COASTAL UPWELLING AND LINK WITH THE GUINEA CURRENT DETACHMENT

(i) Spatial distributions of annual-mean and major upwelling season mean temperature

The maps of the annual-mean SST in the Gulf of Guinea, for the reference and NogradU experiments, are given in Figs. 8a and 8b. The SST minimum observed south of 2°N, signature of the Atlantic cold tongue, remain almost unchanged between the two simulations. The path of the Guinea Current appears warmer between 3° and 5°N in the NogradU experiment. This might be due to larger intrusion of warm waters by the Guinea Current and reduced exchanges with the Atlantic cold tongue in absence of TIWs.

The most striking differences are found between 4°N and the coast, east of Cape Palmas. Here, the minimum temperature zone observed east of Cape Palmas in the reference experiment has completely disappeared. The SST, with a value of 25.8°C between 7.5° and 6°W in the reference experiment, now reaches 27.8°–27.6°C in absence of inertial effects. East of Cape Three Points, only small changes in temperature are observed. SST differences between the two simulations do not here exceed 0.5°C.

Figures 8c and 8d present the SST in the region during the major upwelling season (July–August–September) for the reference and NogradU experiments. Obviously, during this season, the differences between the signatures of the upwelling event east of Cape Palmas and east of Cape Three Points are more visible. Indeed, east of Cape of Palmas, the 25°C isotherm is no more present, and differences of 2.6°C are observed (Fig. 8d). Even in the core of the upwelling season, the surface signature of upwelling vanishes almost entirely. This is not the case east of Cape Three Points, where the 25°C isotherm is still present.

(ii) Seasonal variability of temperature and thermocline depth

These findings are corroborated by the seasonal cycle of SST (Fig. 9) and thermocline depth (Figs. 10b,c, 11a, b). As described in section 3b, the upwelling signature is marked by water below 25°C downstream of the two capes between June and October (Fig. 3a). When nonlinear terms are removed, and thus the Guinea Current is trapped at the coast, coastal upwelling is still present east of Cape Three Points (Fig. 9). East of Cape Palmas, between 7.7° and 4°W, the upwelling has disappeared

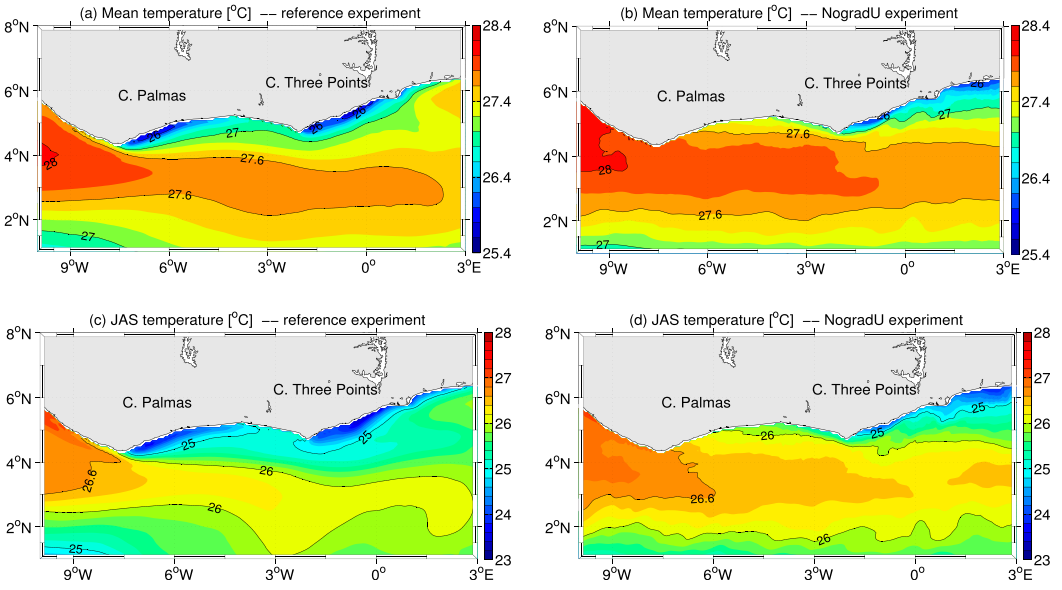

FIG. 8. (top) Maps of spatial distributions of the annual-mean SST (°C) and (bottom) the major cold season (JAS) temperature (°C) in the northern Gulf of Guinea, for (a),(c) the reference experiment and (b),(d) the idealized experiment. The contour interval is 0.2°C.

almost completely. SST does not go below 25.5°C. The detachment of the Guinea Current appears to be the cause of this upwelling.

Although it is not the main focus of our study, we can also note that the minor upwelling in February–April east of Cape Palmas has also disappeared, while there are still colder waters east of Cape Three Points. This suggests that the minor and the major coastal upwelling are both strongly related to the Guinea Current detachment and nonlinear dynamics.

Figure 10a presents the Ekman transport and the model-derived vertical velocities at 20 m (corresponding to the base of the surface mixed layer; see Fig. 10b) for the reference and the idealized experiments. To allow a direct comparison with the results of Bakun (1978), they are averaged over 1° from the shore. The vertical velocities of the NogradU experiment had to be filtered by a 5-points alongshore running mean because of the presence of noise due to the absence of explicit horizontal turbulent viscosity in the momentum equations (Gruber et al. 2011; José et al. 2016). In most of the ROMS model simulations, we rely on the dissipative properties of the third-order upstream advection scheme to filter the grid-scale noise. As explained by Gruber et al. (2011), this is absent in NogradU since we did not add any explicit horizontal turbulent viscosity for consistency.

The Ekman offshore transport is on average negative west of Cape Palmas and positive from the east of Cape Palmas to 3°E. Figure 10a confirms the importance of the detachment of the Guinea Current past Cape Palmas for the presence of upwelling and the dominance of the wind-driven upwelling east of Cape Three Points. For the reference experiment, vertical velocities are particularly large (up to 4.2 m day^{-1}) off Cape Palmas due to the current detachment past the cape and are almost zero farther east. They increase again, following the Ekman offshore transport, east of Cape Three Points. In

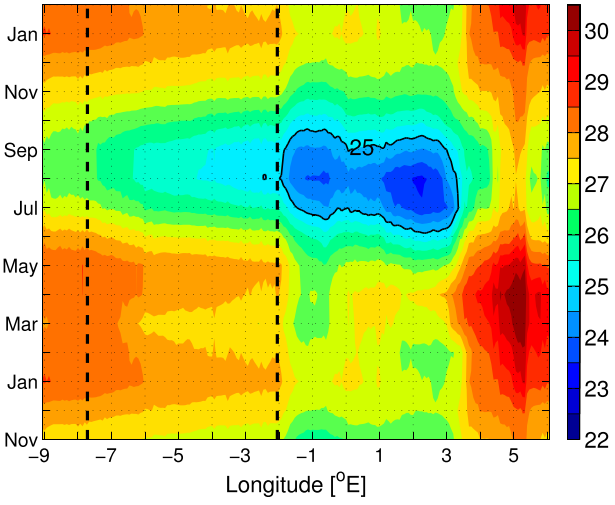

FIG. 9. Longitude–time SST (°C) diagram for the idealized experiment, along the coast (the first grid points in the ocean are around 7 km), in the northern Gulf of Guinea from 9°W to 6°E. The contour interval is 0.5°C. The dashed black line at 7.7°W (2°W) represents the longitude of Cape Palmas (Cape Three Points). The time axis in months extends from November to February.

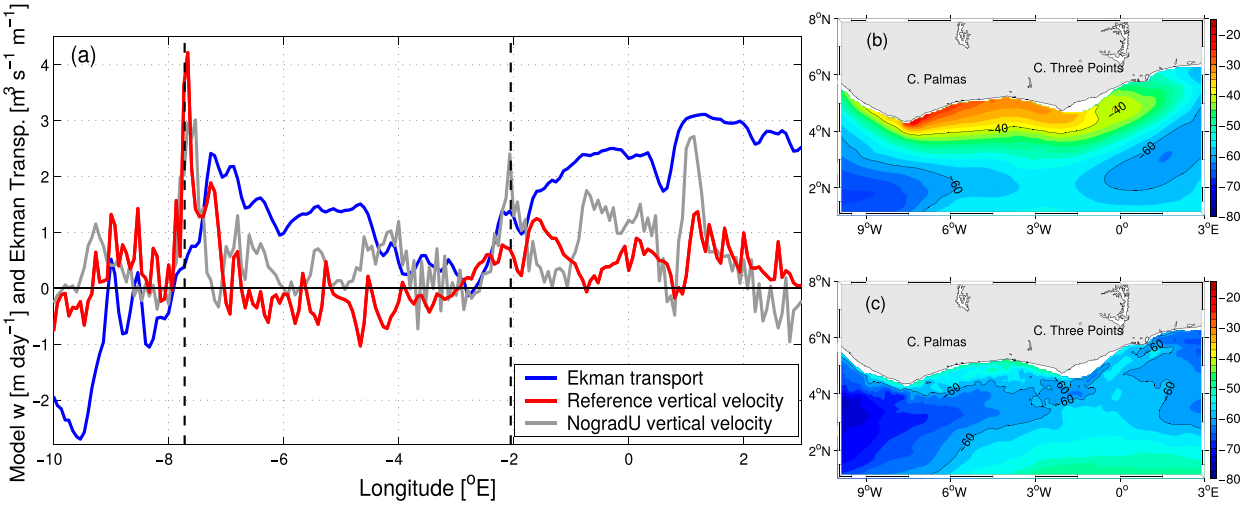

FIG. 10. (a) Offshore Ekman transport ($m^3\,s^{-1}\,m^{-1}$; blue), model-derived vertical velocities ($m\,day^{-1}$) for the reference experiment (red) and model-derived vertical velocities ($m\,day^{-1}$) for the idealized experiment (gray) during the major cold season (JAS), averaged over 1° from the shore. The model-derived vertical velocities are extracted at 20 m. The dashed black line at 7.7° W (2°W) represents the longitude of Cape Palmas (Cape Three Points). Maps of spatial distributions of the major cold season thermocline depth (m) in the northern Gulf of Guinea, for (b) the reference experiment and (c) the idealized experiment. The contour interval is 2.5 m. The isolines −40 and −60 m are represented in black solid lines.

the NogradU experiment, vertical velocities show a weaker maximum at Cape Palmas (illustrating local geostrophic adjustment and local wind effects past the cape) and are roughly following the Ekman offshore transport pattern from 7°W to 1°E.

In addition, the shoaling of the thermocline is also a common measurement for the presence of upwelling. Figures 10b and 10c present the depth of the thermocline during the major upwelling season for the reference (Fig. 10b) and NogradU (Fig. 10c) experiments. The thermocline depth is represented by the depth of the 20°C isotherm (Hughes 1981; Houghton 1983; Gourdeau et al. 2000). The thermocline is shallower in the east of Cape Palmas than in the east of Cape Three Points (Fig. 10b). We note that the thermocline is in general deeper along the coast in the NogradU simulation. Between 1° and 4°N, the thermocline remains almost at the same depth (around 60-m depth; Fig. 10b). The main difference between these experiments is found along the coast.

Furthermore, Figs. 11a and 11b show the seasonal variations of the thermocline depth for the reference experiment (Fig. 11a) and NogradU experiment (Fig. 11b). The thermocline is also in general deeper along the coast in the NogradU simulation. In JAS, during the major upwelling season, the thermocline is around 20–30-m depth east of Cape Palmas in the reference simulation, while it is around 40–50-m depth in the NogradU experiment. More relevant, we can note that between 7° and 6°W, where cooling is usually the most intense (in the reference experiment), the deepening of the thermocline is the strongest. A deepening is also noticeable between the reference and NogradU experiments east of Cape Three Points but with weaker amplitude. It reflects the SST decrease observed at the surface in the east of Cape Palmas.

Thus, the effects of the Guinea Current detachment, brought to light by the canceling of advection of momentum, are important east of Cape Palmas, where the surface signature of the major coastal upwelling does not appear anymore. On the contrary, these effects are weak east of Cape Three Points, where the coastal upwelling event, although slightly weaker, is still present.

(iii) The vorticity equation balance

The vertical pumping derived from the vertically integrated vortex stretching term is illustrated in Fig. 12. This diagnostic has been derived from an integrated vorticity equation [obtained from the model tendency terms and averaged in time for the cold season from years 4 to 9; Eq. (4)]:

$$\underbrace{w_{-h}}_{\text{Pumping}} = \underbrace{-\frac{\beta}{f}\int_{-h}^{\zeta} v\,dz}_{\beta\text{ term}} - \underbrace{\frac{1}{f}\nabla\times\int_{-h}^{\zeta} u\nabla u\,dz}_{\text{Advection}} + \underbrace{\frac{\nabla\times\tau}{\rho_o f}}_{\text{Wind stress curl}}, \tag{4}$$

where w_{-h} is the vertical pumping at the base of the layer (of thickness $h = 20$ m), f is the Coriolis parameter

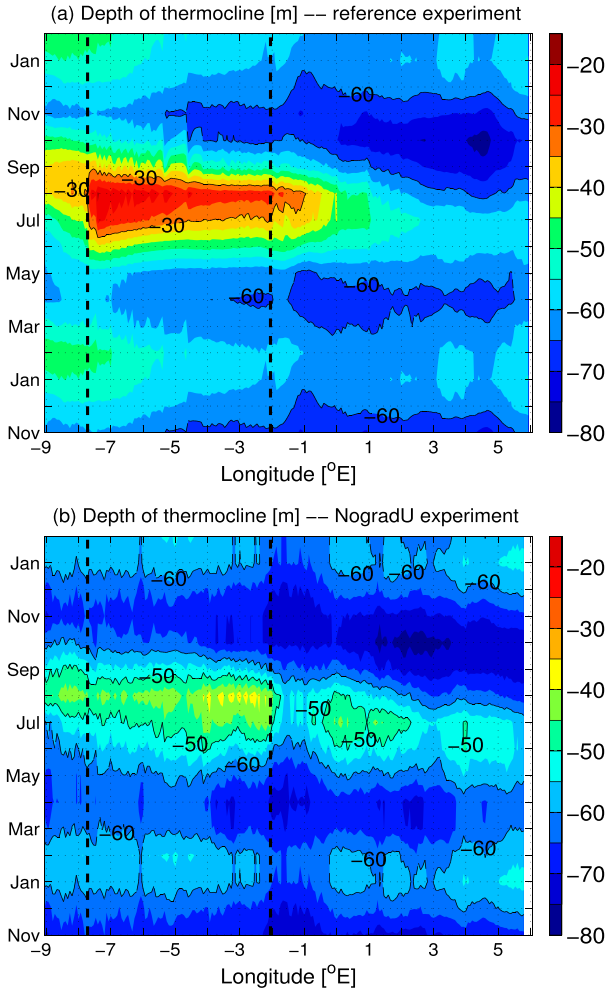

FIG. 11. Longitude–time diagrams of the thermocline depth (m) along the coast (the first grid points in the ocean are around 7 km) in the northern Gulf of Guinea, from 9°W to 6°E, for (a) the reference experiment and (b) the idealized experiment. The contour interval is 5 m. The dashed black line at 7.7°W (2°W) represents the longitude of Cape Palmas (Cape Three Points). The time axis in months extends from November to February.

and β its meridional derivative, and ζ is the free-surface elevation. The terms u and v ($\mathrm{m\,s^{-1}}$) are the zonal and the meridional components of the flow, z (m) is the vertical direction in the Cartesian coordinate system, τ is the alongshore wind stress component ($\mathrm{N\,m^{-2}}$), and ρ_o ($1025\,\mathrm{kg\,m^{-3}}$) is the reference density.

For consistency with the previous section, the vorticity equation is integrated from 20 m to the surface. Figure 12a presents the mean, summer, modeled, vertical velocities at 20 m. They are in close correspondence with the reconstructed vertical pumping from Eq. (4) (Fig. 12b, correlation = 0.81 over the region 1°–7°N and 10°W–2°E). Figure 12c shows unambiguously that advection of momentum is the main contributor of vertical pumping (here more than $6\,\mathrm{m\,day^{-1}}$) off Cape Palmas, while wind stress curl is mostly forcing downwelling (Fig. 12e). The contribution of advection of momentum is weaker off Cape Three Points, with here a faint upwelling contribution from the wind stress curl. Offshore of the Guinea Current (between 8°W and 0° and between 2° and 4°N), the balance is dominated by an equilibrium between advection and beta effect (Figs. 12c and 12d) with weak vertical pumping.

In summary, the findings of these analyses mainly show that two changes are marked when inertial terms are removed: (i) the spatial structure of the Guinea Current is different as the Guinea Current is no more detached from the coast, (ii) the coastal upwelling east of Cape Palmas disappears unlike the one east of Three Points, and (iii) the advection of momentum is the main contributor of vertical pumping off Cape Palmas, while the contribution of this term is weaker off Cape Three Points.

4. Discussion and conclusions

Several hypotheses have been put forward in the past to explain the presence of coastal upwelling in the northern Gulf of Guinea: wind-driven upwelling, effects of eddies, presence of the Guinea Current, and/or remote influence of equatorial dynamics (Ingham 1970; Marchal and Picaut 1977; Bakun 1978; Clarke 1979; Servain et al. 1982; Picaut 1983; Colin 1988, 1991; Colin et al. 1993; Roy 1995; Binet 1997). So far, no definite explanation exists for the presence of this upwelling. This paper presents the results of an ocean model to test if the coastal upwelling in the northern Gulf of Guinea is a consequence of detachment of the Guinea Current from the coast and of local winds.

After assessing the quality of a realistic reference experiment in reproducing the known aspects of the circulation and hydrology in the region, a sensitivity experiment in which advection of momentum is canceled is performed. As seen in other parts of the World Ocean (Chao et al. 1996; José 2013; José et al. 2016), these nonlinear terms are responsible for the detachment of the Guinea Current from the coast. Although the advection of momentum affects the large-scale ocean dynamics [e.g., the EUC (Wacongne 1989)], the general patterns of the large-scale circulation (i.e., the westward-flowing SEC and the eastward-flowing NECC) and hydrology are still present in the NoGradU experiment. In this case, the Atlantic cold tongue is more intense and extends to the west of the basin. These changes in the center of the basin when advection of momentum has been canceled could be attributed to the absence of the TIWs, which contribute to warm up the Atlantic cold tongue (Menkès et al. 2002; Athié et al. 2009).

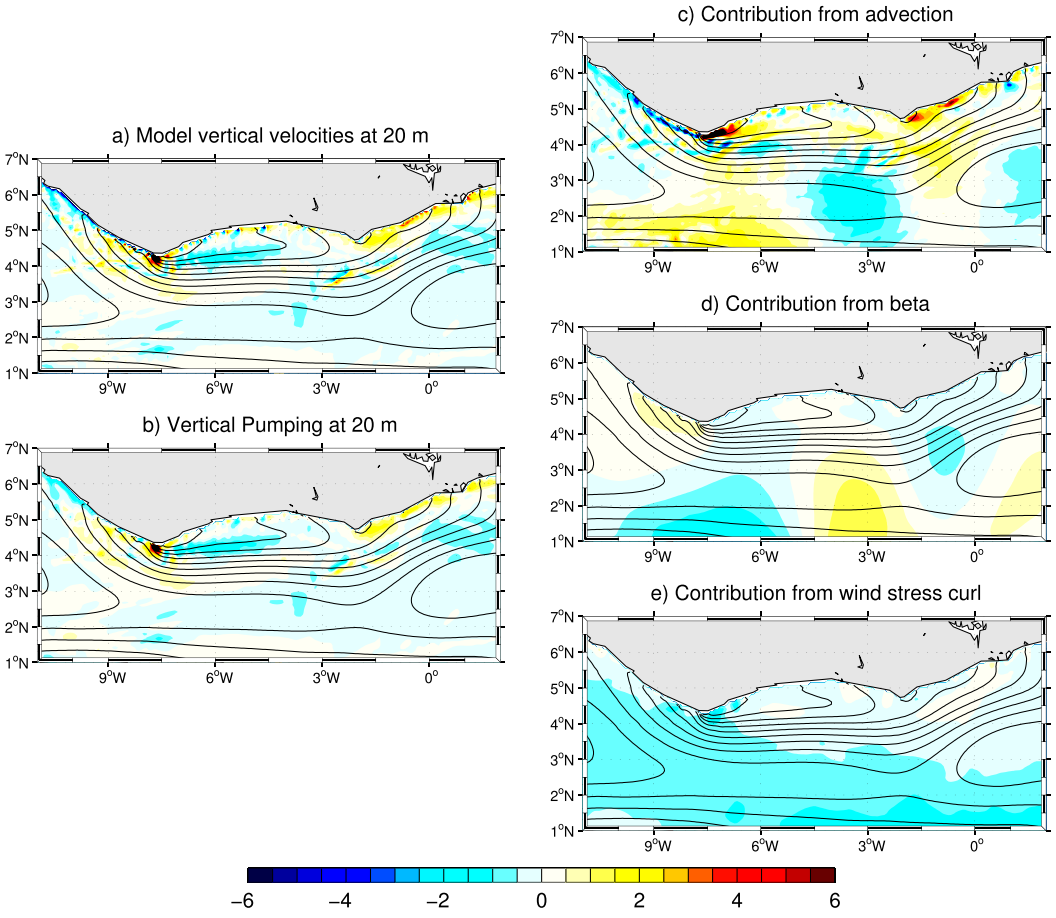

FIG. 12. (a) Model mean summer vertical velocities at 20 m (m day^{-1}), (b) reconstructed vertical pumping (m day^{-1}), and (c),(d),(e) its contributions (m day^{-1}) from a vorticity balance on a surface layer of 20 m over the summer months for 6 yr of the reference experiment. Black contours (1 cm contour interval) represent the mean free-surface elevation for this season. The terms of the vorticity balance are the advection of vorticity in (c), the beta effect in (d), and the wind stress curl in (e) [see Eq. (4)].

In the northern Gulf of Guinea, the spatial structure of the Guinea Current is substantially modified by the absence of advection of momentum in the NoGradU experiment. In the reference experiment (and in the observations), the Guinea Current shows a broad extension over 200 km from the coast. Without the advection of momentum, the Guinea Current is now confined in a narrow band close to the coast with increased velocities and is controlled by bottom topography. As the Guinea Current is no more detached from the coast, these results suggest that the dynamics of the Guinea Current depends strongly on the inertial terms.

Figure 12 shows that the offshore side is controlled by a balance between advection of vorticity and beta. This is in agreement with the inertial boundary layer along a northern wall proposed by Fofonoff (1954). The thickness of the boundary layer is here defined by the balance between advection of vorticity and beta: $\delta_I = (U/\beta)^{1/2}$, using $U = 1\,\mathrm{m\,s^{-1}}$ for the Guinea Current and $\beta = 2.3 \times 10^{-11}$ at 5°N. We obtain $\delta_I = 210$ km, which corresponds approximately to the width of the Guinea Current (see Fig. 1). This also confirms the argument of Picaut (1983), who was questioning the suitability of the use of linear (i.e., without advection of momentum) numerical models to address the ocean dynamics and the coastal upwelling in the region (Clarke 1979; Moore et al. 1978).

In relation to the nondetachment of the Guinea Current from the coast, the absence of the isotherm 25°C east of Cape Palmas, the seasonal cycle of the SST, and the deepening of the thermocline east of Cape Palmas indicate that (i) there are no more cold waters upwelled east of Cape Palmas and that (ii) a cooling of surface water is still present east of Cape Three Points. These results suggest that two different mechanisms are involved for the coastal upwelling east of Cape Palmas and east of Cape Three Points.

East of Cape Palmas, the absence of momentum advection in the NoGradU experiment results in the total disappearance of the surface signature of coastal upwelling. Hence, the upwelling of Cape Palmas can be explained by the nonlinear dynamics of the Guinea Current and its detachment from the coast. Several examples exist in western boundary currents of the existence of upwelling driven by the detachment of a current over a widening shelf. This is the case, for example, south of Madagascar (Lutjeharms and Machu 2000; Machu et al. 2002; José et al. 2016), east of Australia (Oke and Middleton 2000), and in northeastern Florida (Janowitz and Pietrafesa 1982). Janowitz and Pietrafesa (1982) show how an inertial flow above a varying topography can create upwelling. The effects of inertia for the current driving upwelling south of Madagascar have been illustrated by José et al. (2016). It appears that the same process is occurring in the Gulf of Guinea. Ingham (1970) has proposed that the upwelling could be related to a shallowing of the thermocline between March and July. This shallowing of the thermocline is induced by geostrophic adjustment across the Guinea Current. In the NoGradU experiment, although trapped to the shore, the Guinea Current still exists and still follows a geostrophic balance. This shows that the rising of isopycnals associated with the geostrophic balance is not sufficient for the presence of upwelling.

The mechanism of a coastal upwelling induced by the effects of inertia on the Guinea Current detachment is supported and consistent with the work of Colin (1988). For this author, the latitudinal extension of the Guinea Current would be the cooling mechanism east of Cape Palmas. He showed that the variability of SST for coastal stations of Côte d'Ivoire was related to the intensity and the latitudinal extension of the Guinea Current. His study also revealed that the thermocline is closer to the surface at the coast in boreal summer, when the Guinea Current is located offshore and not confined only to the continental shelf (as in the NogradU experiment). Therefore, it appears that the upwelling of Cape Palmas is explained by the nonlinear dynamics of the Guinea Current and its detachment from the coast.

The results of the Ekman offshore transport and the model-derived vertical velocities analysis give additional information about the coastal upwelling dynamics. Indeed, it shows how the detachment of the Guinea Current past Cape Palmas is able to create locally strong vertical velocities. The NogradU experiment is still producing positive vertical velocities, but they are not sufficient to create a significant surface upwelling signature. The importance of the detachment of the Guinea Current past Cape Palmas for the presence of upwelling and the dominance of the wind-driven upwelling east of Cape Three Points are proven. The inertial effects and topographic variations result in important vertical velocities past Cape Palmas, as for the northeastern Florida upwelling (Janowitz and Pietrafesa 1982).

Furthermore, a vorticity balance obtained from the model tendency terms gives us confidence in these results. The advection of momentum is the main contributor of vertical pumping off Cape Palmas, while the contribution of this term is weaker off Cape Three Points. The wind stress curl is mostly forcing downwelling east of Cape Palmas and a slight upwelling contribution is found east of Cape Three Points. This confirms that the upwelling off Cape Palmas is explained by pumping through balance with the advective terms. This upwelling is due to vertical pumping, induced by advection of momentum in an equivalent manner as derived by Janowitz and Pietrafesa [1982, see their Eq. (11)]; advection of vorticity associated with the geostrophic flow results in a divergence and vertical pumping at first order.

For the case of the upwelling that is still present east of Cape Three Points in the NoGradU experiment, the analysis of seasonal patterns of SST, Ekman transport divergence, and the vorticity balance indicates that this cooling may be linked to local wind effects: Ekman transport coastal divergence (Fig. 10a) and a slight contribution of Ekman pumping induced by wind stress curl (Fig. 12e). The Ghanaian coast presents a more meridional coastal trend and thus is more parallel to the winds (Toualy et al. 2012). Indeed, the shelf bathymetry is different between the two capes, as showed in Fig. 7. The continental shelf east of Cape Three Points is wider than the one east of Cape Palmas. The response of the water temperature to the same upwelling-favorable wind stress could be different between the two capes. The temperature response is more rapid east of Cape Palmas, where the thermocline is shallower (Fig. 10b; Fig. 11a) for upwelling-favorable wind stress. However, because of the coastline orientation and the wind stress direction, the wind stress around Cape Palmas is less upwelling favorable than the wind stress around Cape Three Points. The values of Ekman transport divergence are significant and can induce cooling east of Cape Three Points, even if we found that the maximum wind-driven velocity is located 300 km east of the colder surface waters, as reported by Bakun (1978). This might be due to the presence of the cape. Figure 10 shows that although this is smaller than at Cape Palmas, there is still an effect of the cape on upwelling at Cape Three Points.

This work highlights the importance of inertial terms on ocean dynamics in the Gulf of Guinea. To our knowledge, the inertia effect on this eastern part of the tropical Atlantic has not been documented yet. Indeed, Picaut (1983) questioned the adequacy of linear numerical models to explain the generation process of

coastal upwelling in this region. These models do not take into account the nonlinear advection terms (Clarke 1979; Moore et al. 1978).

From the list of possible explanations for coastal upwelling in the Gulf of Guinea (wind-driven upwelling, effects of eddies, presence of the Guinea Current, and remote influence of equatorial dynamics), Djakouré et al. (2014) were able to rule out the effects of capes and eddies as a cause for upwelling. In their model simulation, upwelling was still occurring in the absence of capes and in the absence of the cyclonic eddies generated east of them. Here, it is now possible to highlight

- the detachment of the Guinea Current from the coast (Colin 1988) and the advection of vorticity associated with the geostrophic flow, resulting in a divergence and vertical pumping at first order as the principal mechanism explaining coastal upwelling east of Cape Palmas; and
- the wind-driven upwelling explaining cold, upwelled waters east of Cape Three Points, as suggested by Bakun (1978), Adamec and O'Brien (1978), and Toualy et al. (2012).

Now, further investigation would be needed to determine the potential effects of the coastal-trapped Kelvin waves of equatorial origin. Although such waves cannot be fully responsible for upwelling (since upwelling already occurs in an adjusted climatology experiment such as described here), they could modulate the signal by rising and lowering the thermocline.

Acknowledgments. We acknowledge funding from the EU FP7/2007-2013 under Grant Agreement 603521, project PREFACE. The research leading to these results also received funding from the French Institut de Recherche pour le Développement (IRD). Simulations were performed at Institut Français de Recherche pour l'Exploitation de la Mer (IFREMER, Brest, France) with the computing facility CAPARMOR. The authors acknowledge the authors of the data made available in free access and used in this study. The SST MODIS data are provided by the Ocean Biology Processing Group at the GSFC, Greenbelt, Maryland, 20771, and the CARS 2009 data are available online (at www.cmar.csiro.au/cars). The altimeter products were produced by Ssalto/Duacs and distributed by AVISO, with support from CNES (http://www.aviso.oceanobs.com/duacs/). The authors thank the editor and the anonymous reviewers for their helpful comments and suggestions for this manuscript.

REFERENCES

Adamec, D., and J. J. O'Brien, 1978: The seasonal upwelling in the Gulf of Guinea due to remote forcing. *J. Phys. Oceanogr.*, **8**, 1050–1060, doi:10.1175/1520-0485(1978)008<1050:TSUITG>2.0.CO;2.

Allen, S. E., and B. M. Hickey, 2010: Dynamics of advection-driven upwelling over a shelf break submarine canyon. *J. Geophys. Res.*, **115**, C08018, doi:10.1029/2009JC005731.

Arfi, R., O. Pezennec, S. Cissoko, and M. Mensah, 1991: Variations spatiale et temporelle de la résurgence ivoiro-ghanéenne. *Pêcheries Ouest-Africaines Variabilité, Instabilité et Changement*, P. Cury and C. Roy, Eds., ORSTOM, 162–172.

Arnault, S., 1987: Tropical Atlantic geostrophic currents and ship drifts. *J. Geophys. Res.*, **92**, 5076–5088, doi:10.1029/JC092iC05p05076.

Athié, G., F. Marin, A.-M. Tréguier, B. Bourlès, and C. Guiavarc'h, 2009: Sensitivity of near-surface tropical instability waves to submonthly wind forcing in the tropical Atlantic. *Ocean Modell.*, **30**, 241–255, doi:10.1016/j.ocemod.2009.06.016.

Bakun, A., 1973: Coastal upwelling indices, west coast of North America 1946-71. NOAA Tech. Rep. NMFS SSRF-671, 112 pp.

——, 1978: Guinea Current upwelling. *Nature*, **271**, 147–150, doi:10.1038/271147a0.

——, and C. S. Nelson, 1991: The seasonal cycle of wind-stress curl in subtropical eastern boundary current regions. *J. Phys. Oceanogr.*, **21**, 1815–1834, doi:10.1175/1520-0485(1991)021<1815:TSCOWS>2.0.CO;2.

Binet, D., 1997: Climate and pelagic fisheries in the Canary and Guinea Currents 1964-1993: The role of trade winds and the Southern Oscillation. *Oceanol. Acta*, **20**, 177–190.

Blayo, E., and L. Debreu, 1999: Adaptive mesh refinement for finite-difference ocean models: First experiments. *J. Phys. Oceanogr.*, **29**, 1239–1250, doi:10.1175/1520-0485(1999)029<1239:AMRFFD>2.0.CO;2.

Bourlès, B., R. L. Molinari, E. Johns, W. Wilson, and K. Leaman, 1999: Upper layer currents in the western tropical North Atlantic. *J. Geophys. Res.*, **104**, 1361–1376, doi:10.1029/1998JC900025.

Boyer, D., and L. Tao, 1987: On the motion of linearly stratified rotating fluids past capes. *J. Fluid Mech.*, **180**, 429–449, doi:10.1017/S0022112087001885.

Caniaux, G., H. Giordani, J.-L. Redelsperger, F. Guichard, E. Key, and M. Wade, 2011: Coupling between the Atlantic cold tongue and West African monsoon in boreal spring and summer. *J. Geophys. Res.*, **116**, C04003, doi:10.1029/2010JC006570.

Chao, Y., A. Gangopadhyay, F. O. Bryan, and W. R. Holland, 1996: Modeling the Gulf Stream System: How far from reality? *Geophys. Res. Lett.*, **23**, 3155–3158, doi:10.1029/96GL03003.

Charney, J., 1955: The generation of ocean currents by wind. *J. Mar. Res.*, **14**, 477–498.

Clarke, A., 1979: On the generation of the seasonal coastal upwelling in the Gulf of Guinea. *J. Geophys. Res.*, **84**, 3743–3751, doi:10.1029/JC084iC07p03743.

Colin, C., 1988: Coastal upwelling events in front of the Ivory Coast during the FOCAL program. *Oceanol. Acta*, **11**, 125–138.

——, 1991: Sur les upwellings équatorial et côtier (5°N) dans le Golfe de Guinée. *Oceanol. Acta*, **14**, 223–240.

——, Y. Gallardo, R. Chuchla, and S. Cissoko, 1993: Environnements climatique et océanographique sur le plateau continental de Côte d'Ivoire. *Environnement et Ressources aquatiques de Côte d'Ivoire: 1. Le Milieu Marin*, P. Le Loeuff, E. Marchal, and J. Amon Kothias, Eds., ORSTOM, 75–110.

Crépon, M., C. Richez, and M. Chartier, 1984: Effects of coastline geometry on upwellings. *J. Phys. Oceanogr.*, **14**, 1365–1382, doi:10.1175/1520-0485(1984)014<1365:EOCGOU>2.0.CO;2.

Cury, P., and C. Roy, 2002: Environmental forcing and fisheries resources in Côte d'Ivoire and Ghana: Did something happen?

Environmental Forcing and Sustainable Development of Marine Resources, J. M. McGlade et al., Eds., Vol. 11, *The Gulf of Guinea Large Marine Ecosystem*, Elsevier, 241–260.

Da Silva, A., C. Young, and S. Levitus, 1994: *Algorithms and Procedures*. Vol. 1, *Atlas of Surface Marine Data 1994*, NOAA Atlas NESDIS 6, 83 pp.

Debreu, L., and E. Blayo, 2008: Two-way embedding algorithms: A review. *Ocean Dyn.*, **58**, 415–428, doi:10.1007/s10236-008-0150-9.

——, P. Marchesiello, P. Penven, and G. Cambon, 2012: Two-way nesting in split-explicit ocean models: Algorithms, implementation and validation. *Ocean Modell.*, **49–50**, 1–21, doi:10.1016/j.ocemod.2012.03.003.

Djakouré, S., P. Penven, B. Bourlès, J. Veitch, and V. Koné, 2014: Coastally trapped eddies in the north of the Gulf of Guinea. *J. Geophys. Res. Oceans*, **119**, 6805–6819, doi:10.1002/2014JC010243.

Ducet, N., P. Y. L. Traon, and G. Reverdin, 2000: Global high-resolution mapping of ocean circulation from TOPEX/Poseidon and ERS-1 and -2. *J. Geophys. Res.*, **105**, 19 477–19 498, doi:10.1029/2000JC900063.

Dufois, F., P. Penven, C. P. Whittle, and J. Veitch, 2012: On the warm nearshore bias in Pathfinder monthly SST products over eastern boundary upwelling systems. *Ocean Modell.*, **47**, 113–118, doi:10.1016/j.ocemod.2012.01.007.

Dunn, J. R., and K. R. Ridgway, 2002: Mapping ocean properties in regions of complex topography. *Deep-Sea Res. I*, **49**, 591–604, doi:10.1016/S0967-0637(01)00069-3.

Durski, S. M., R. Samelson, J. Allen, and G. D. Egbert, 2008: Normal-mode instabilities of a time-dependent coastal upwelling jet. *J. Phys. Oceanogr.*, **38**, 2056–2071, doi:10.1175/2008JPO3803.1.

Enriquez, A. G., and C. A. Friehe, 1995: Effects of wind stress and wind stress curl variability on coastal upwelling. *J. Phys. Oceanogr.*, **25**, 1651–1671, doi:10.1175/1520-0485(1995)025<1651:EOWSAW>2.0.CO;2.

Fofonoff, N. P., 1954: Steady flow in a frictionless homogeneous ocean. *J. Mar. Res.*, **13**, 254–262.

Garzoli, S. L., and E. J. Katz, 1983: The forced annual reversal of the Atlantic North Equatorial Countercurrent. *J. Phys. Oceanogr.*, **13**, 2082–2090, doi:10.1175/1520-0485(1983)013<2082:TFAROT>2.0.CO;2.

Gourdeau, L., J. Verron, T. Delcroix, A. J. Busalacchi, and R. Murtugudde, 2000: Assimilation of TOPEX/Poseidon altimetric data in a primitive equation model of the tropical Pacific Ocean during the 1992–1996 El Niño-Southern Oscillation period. *J. Geophys. Res.*, **105**, 8473–8488, doi:10.1029/2000JC900011.

Gruber, N., Z. Lachkar, H. Frenzel, P. Marchesiello, M. Munnich, J. C. McWilliams, T. Nagai, and G.-K. Plattner, 2011: Eddy-induced reduction of biological production in eastern boundary upwelling systems. *Nat. Geosci.*, **4**, 787–792, doi:10.1038/ngeo1273.

Gu, G., and R. Adler, 2004: Seasonal evolution and variability associated with the African monsoon system. *J. Climate*, **17**, 3364–3377, doi:10.1175/1520-0442(2004)017<3364:SEAVAW>2.0.CO;2.

Hardman-Mountford, N. J., and J. M. McGlade, 2003: Seasonal and interannual variability of oceanographic processes in the Gulf of Guinea: An investigation using AVHRR sea surface temperature data. *Int. J. Remote Sens.*, **24**, 3247–3268, doi:10.1080/0143116021000021297.

Houghton, R. W., 1983: Seasonal variations of the subsurface thermal structure in the Gulf of Guinea. *J. Phys. Oceanogr.*, **13**, 2070–2081, doi:10.1175/1520-0485(1983)013<2070:SVOTST>2.0.CO;2.

Hsueh, Y., and J. J. O'Brien, 1971: Steady coastal upwelling induced by an alongshore current. *J. Phys. Oceanogr.*, **1**, 180–186, doi:10.1175/1520-0485(1971)001<0180:SCUIBA>2.0.CO;2.

Hughes, R. L., 1981: The influence of thermocline slope on equatorial thermocline displacement. *Dyn. Atmos. Oceans*, **5**, 147–157, doi:10.1016/0377-0265(81)90008-7.

Ingham, M., 1970: Coastal upwelling in the northwestern Gulf of Guinea. *Bull. Mar. Sci.*, **20**, 1–34.

Janowitz, G. S., and L. J. Pietrafesa, 1982: The effects of alongshore variation in bottom topography on a boundary current (topographically induced upwelling). *Cont. Shelf Res.*, **1**, 123–141, doi:10.1016/0278-4343(82)90001-2.

José, Y., 2013: Mesoscale structuring of the pelagic ecosystem in the Mozambique Channel: A modelling approach. Ph.D. thesis, University of Cape Town, 194 pp. [Available from University of Cape Town, Rondebosch, Cape Town, 7700, South Africa.]

——, P. Penven, O. Aumont, E. Machu, C. Moloney, F. Shillington, and O. Maury, 2016: Suppressing and enhancing effects of mesoscale dynamics on biological production in the Mozambique Channel. *J. Mar. Syst.*, **158**, 129–139, doi:10.1016/j.jmarsys.2016.02.003.

Jouanno, J., F. Marin, Y. D. Penhoat, J.-M. Molines, and J. Sheinbaum, 2011: Seasonal modes of surface cooling in the Gulf of Guinea. *J. Phys. Oceanogr.*, **41**, 1408–1416, doi:10.1175/JPO-D-11-031.1.

Katz, E., and S. Garzoli, 1982: Response of the western equatorial Atlantic Ocean to an annual wind cycle. J. *Mar. Res.*, **40**, 307–327.

Kolodziejczyk, N., 2008: Analyse de la circulation de subsurface et de sa variabilité dans le Golfe de Guinée. Ph.D. thesis, Thèse de doctorat de l'Université de Bretagne, 256 pp. [Available from Université de Bretagne, 3 Rue des Archives, 29238 Brest, France.]

Koranteng, K., and J. M. McGlade, 2001: Climatic trends in continental shelf waters off Ghana and in the Gulf of Guinea, 1963–1992. *Oceanol. Acta*, **24**, 187–198, doi:10.1016/S0399-1784(01)01140-9.

Large, W. G., J. C. McWilliams, and S. C. Doney, 1994: Oceanic vertical mixing: A review and a model with a nonlocal boundary layer parameterization. *Rev. Geophys.*, **32**, 363–403, doi:10.1029/94RG01872.

Lemasson, L., and J. Rébert, 1973: Circulation dans le Golfe de Guinée: Etude de la région d'origine du sous-courant ivoirien. *Cah. ORSTOM, Ser. Oceanogr.*, **11**, 303–316.

Longhurst, A. R., 1962: A review of the oceanography of the Gulf of Guinea. *Bull. Inst. Fr. Afr. Noire*, **24**, 633–663.

Lumpkin, R., and G. Johnson, 2013: Global ocean surface velocities from drifters: Mean, variance, El Niño–Southern Oscillation response, and seasonal cycle. *J. Geophys. Res. Oceans*, **118**, 2992–3006, doi:10.1002/jgrc.20210.

Lutjeharms, J. R. E., and E. Machu, 2000: An upwelling cell inshore of the East Madagascar Current. *Deep-Sea Res. I*, **47**, 2405–2411, doi:10.1016/S0967-0637(00)00026-1.

Machu, E., J. R. E. Lutjeharms, A. M. Webb, and H. M. V. Aken, 2002: First hydrographic evidence of the southeast Madagascar upwelling cell. *Geophys. Res. Lett.*, **29**, 2009, doi:10.1029/2002GL015381.

Marchal, E., and J. Picaut, 1977: Répartition et abondance évaluées par écho-integration des poissons du plateau ivoiro-ghanéen en relation avec les upwellings locaux. *J. Rech. Oceanogr.*, **2**, 39–58.

Marchesiello, P., and P. Estrade, 2009: Eddy activity and mixing in upwelling systems: A comparative study of northwest Africa

and California regions. *Int. J. Earth Sci.*, **98**, 299–308, doi:10.1007/s00531-007-0235-6.

——, and ——, 2010: Upwelling limitation by onshore geostrophic flow. *J. Mar. Res.*, **68**, 37–62, doi:10.1357/002224010793079004.

——, J. C. McWilliams, and A. Shchepetkin, 2001: Open boundary conditions for long-term integration of regional oceanic models. *Ocean Modell.*, **3**, 1–20, doi:10.1016/S1463-5003(00)00013-5.

——, ——, and ——, 2003: Equilibrium structure and dynamics of the California Current System. *J. Phys. Oceanogr.*, **33**, 753–783, doi:10.1175/1520-0485(2003)33<753:ESADOT>2.0.CO;2.

——, L. Debreu, and X. Couvelard, 2009: Spurious diapycnal mixing in terrain-following coordinate models: The problem and a solution. *Ocean Modell.*, **26**, 156–169, doi:10.1016/j.ocemod.2008.09.004.

Menkès, C., and Coauthors, 2002: A whirling ecosystem in the equatorial Atlantic. *Geophys. Res. Lett.*, **29**, 1553, doi:10.1029/2001GL014576.

Moore, W., P. Hisard, J. McCreary, J. Merle, J. O'Brien, J. Picaut, J. Verstraete, and C. Wunsch, 1978: Equatorial adjustment in the eastern Atlantic Ocean. *Geophys. Res. Lett.*, **5**, 637–640, doi:10.1029/GL005i008p00637.

Oke, P. R., and J. H. Middleton, 2000: Topographically induced upwelling off eastern Australia. *J. Phys. Oceanogr.*, **30**, 512–531, doi:10.1175/1520-0485(2000)030<0512:TIUOEA>2.0.CO;2.

Opoku-Ankomah, Y., and I. Cordery, 1994: Atlantic sea surface temperatures and rainfall variability in Ghana. *J. Climate*, **7**, 551–558, doi:10.1175/1520-0442(1994)007<0551:ASSTAR>2.0.CO;2.

Özgökmen, T. M., E. P. Chassignet, and A. M. Paiva, 1997: Impact of wind forcing, bottom topography, and inertia on midlatitude jet separation in a quasigeostrophic model. *J. Phys. Oceanogr.*, **27**, 2460–2476, doi:10.1175/1520-0485(1997)027<2460:IOWFBT>2.0.CO;2.

Penven, P., C. Roy, A. Colin de Verdiere, and J. Largier, 2000: Simulation of a coastal jet retention process using a barotropic model. *Oceanol. Acta*, **23**, 615–634, doi:10.1016/S0399-1784(00)01106-3.

——, V. Echevin, J. Pasapera, F. Colas, and J. Tam, 2005: Average circulation, seasonal cycle, and mesoscale dynamics of the Peru Current system: A modeling approach. *J. Geophys. Res.*, **110**, C10021, doi:10.1029/2005JC002945.

Philander, S. G. H., 1979: Upwelling in the Gulf of Guinea. *J. Mar. Res.*, **37**, 23–33.

——, and R. C. Pacanowski, 1986: A model of the seasonal cycle in the tropical Atlantic Ocean. *J. Geophys. Res.*, **91**, 14 192–14 206, doi:10.1029/JC091iC12p14192.

Picaut, J., 1983: Propagation of the seasonal upwelling in the eastern equatorial Atlantic. *J. Phys. Oceanogr.*, **13**, 18–37, doi:10.1175/1520-0485(1983)013<0018:POTSUI>2.0.CO;2.

Pringle, J. M., 2002: Enhancement of wind-driven upwelling and downwelling by alongshore bathymetric variability. *J. Phys. Oceanogr.*, **32**, 3101–3112, doi:10.1175/1520-0485(2002)032<3101:EOWDUA>2.0.CO;2.

Richardson, P. L., and D. Walsh, 1986: Mapping climatological seasonal variations of surface currents in the tropical Atlantic using ship drifts. *J. Geophys. Res.*, **91**, 10 537–10 550, doi:10.1029/JC091iC09p10537.

——, and G. Reverdin, 1987: Seasonal cycle of velocity in the Atlantic North Equatorial Countercurrent as measured by surface drifters, current meters, and ship drifts. *J. Geophys. Res.*, **92**, 3691–3708, doi:10.1029/JC092iC04p03691.

Rio, M.-H., S. Guinehut, and G. Larnicol, 2011: New CNES-CLS09 global mean dynamic topography computed from the combination of GRACE data, altimetry, and in situ measurements. *J. Geophys. Res.*, **116**, C07018, doi:10.1029/2010JC006505.

Risien, C. M., and D. B. Chelton, 2008: A global climatology of surface wind and wind stress fields from eight years of QuikSCAT scatterometer data. *J. Phys. Oceanogr.*, **38**, 2379–2413, doi:10.1175/2008JPO3881.1.

Roy, C., 1995: The Côte d'Ivoire and Ghana coastal upwellings: Dynamics and changes. *Dynamics and Use of Sardinella Resources from Upwelling off Ghana and Ivory Coast*, X. Bard and K. A. Koranteng, Eds., ORSTOM, 346–361.

Schott, F. A., J. P. McCreary Jr., and G. C. Johnson, 2004: Shallow overturning circulations of the tropical-subtropical oceans. *Earth's Climate*, *Geophys. Monogr.*, Vol. 147, Amer. Geophys. Union, 261–304.

Schumann, E. H., L.-A. Perrins, and I. T. Hunter, 1982: Upwelling along the south coast of the Cape Province, South Africa. *S. Afr. J. Sci.*, **78**, 238–242.

Servain, J., J. Picaut, and J. Merle, 1982: Evidence of remote forcing in the equatorial Atlantic Ocean. *J. Phys. Oceanogr.*, **12**, 457–463, doi:10.1175/1520-0485(1982)012<0457:EORFIT>2.0.CO;2.

Shchepetkin, A. F., and J. C. McWilliams, 2003: A method for computing horizontal pressure force in an oceanic model with a non-aligned vertical coordinate. *J. Geophys. Res.*, **108**, 3090, doi:10.1029/2001JC001047.

——, and ——, 2005: The Regional Oceanic Modeling System (ROMS): A split-explicit, free-surface, topography-following-coordinate oceanic model. *Ocean Modell.*, **9**, 347–404, doi:10.1016/j.ocemod.2004.08.002.

Song, Y., and D. B. Haidvogel, 1994: A semi-implicit ocean circulation model using a generalized topography-following coordinate system. *J. Comput. Phys.*, **115**, 228–244, doi:10.1006/jcph.1994.1189.

Stramma, L., J. Fischer, P. Brandt, F. Schott, G. Goni, and P. Malanotte-Rizzoli, 2003: Circulation, variability and near-equatorial meridional flow in the central tropical Atlantic. *Interhemispheric Water Exchange in the Atlantic Ocean*, G. J. Goni and P. Rizzoli, Eds., Elsevier Oceanography Series, Vol. 68, Elsevier, 1–22.

Toualy, E., G. Stanojevic, K. Kouadio, and A. Aman, 2012: Multidecadal variability of sea surface temperature in the northern coast of the Gulf of Guinea. *Asian J. Appl. Sci.*, **5**, 552–562, doi:10.3923/ajaps.2012.552.562.

Varlet, F., 1958: Les traits essentiels du régime côtier de l'Atlantique près d'Abidjan (Côte d'Ivoire). *Bull. l'IFAN Sci. Nat.*, **20A**, 1089–1102.

Veitch, J., P. Penven, and F. Shillington, 2009: The Benguela: A laboratory for comparative modeling studies. *Prog. Oceanogr.*, **83**, 296–302, doi:10.1016/j.pocean.2009.07.008.

——, ——, and ——, 2010: Modeling equilibrium dynamics of the Benguela Current system. *J. Phys. Oceanogr.*, **40**, 1942–1964, doi:10.1175/2010JPO4382.1.

Wacongne, S., 1989: Dynamical regimes of a fully nonlinear stratified model of the Atlantic Equatorial Undercurrent. *J. Geophys. Res.*, **94**, 4801–4815, doi:10.1029/JC094iC04p04801.

Wiafe, G., H. B. Yaqub, M. A. Mensah, and C. L. J. Frid, 2008: Impact of climate change on long-term zooplankton biomass in the upwelling region of the Gulf of Guinea. *ICES J. Mar. Sci.*, **65**, 318–324, doi:10.1093/icesjms/fsn042.

Wooster, W. S., and J. J. L. Reid, 1963: Eastern boundary currents. *Physical Oceanography*, M. N. Hill, Eds., The Sea—Ideas and Observations on Progress in the Study of the Seas, Vol. 1, John Wiley and Sons, 253–280.